2 of 3

Office of Naval Research
Department of the Navy
Contract Nonr 220(43)

50-p
$1.25

LINEARIZED THEORY OF A TWO-DIMENSIONAL PLANING FLAT PLATE IN A CHANNEL OF FINITE DEPTH-I

by

D. K. Ai
A. J. Acosta
Z. L. Harrision

Hydrodynamics Laboratory
Kármán Laboratory of Fluid Mechanics and Jet Propulsion
California Institute of Technology
Pasadena, California

Report No. E-110.2

April 1964

DISCLAIMER NOTICE

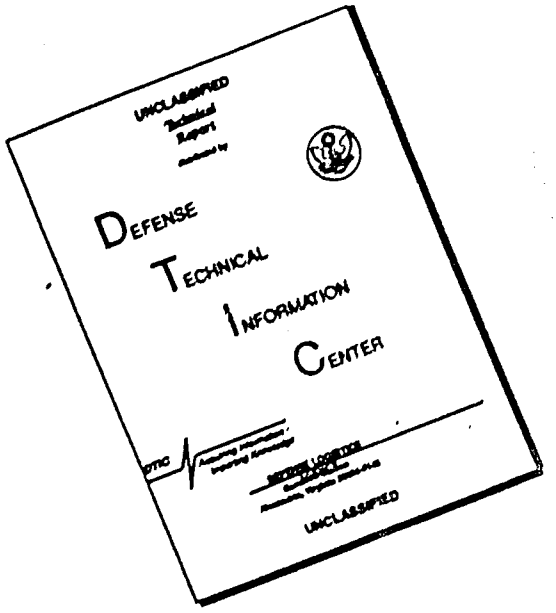

THIS DOCUMENT IS BEST QUALITY AVAILABLE. THE COPY FURNISHED TO DTIC CONTAINED A SIGNIFICANT NUMBER OF PAGES WHICH DO NOT REPRODUCE LEGIBLY.

Office of Naval Research
Department of the Navy
Contract Nonr 220(43)

LINEARIZED THEORY OF A TWO-DIMENSIONAL PLANING FLAT PLATE IN A CHANNEL OF FINITE DEPTH - I

by

D. K. Ai
A. J. Acosta
Z. L. Harrison

Hydrodynamics Laboratory
Karman Laboratory of Fluid Mechanics and Jet Propulsion
California Institute of Technology
Pasadena, California

Report No. 110.2 April 1964

ABSTRACT

Linearized free-streamline theory is used to calculate the spray-sheet thickness and lift-slope for a flat plate, cavitating, two-dimensional hydrofoil in a channel of finite depth with an upper free surface and lower boundary partly free and partly rigid. Only the case of zero cavitation number is considered. Some measurements were made of the submergence of a hydrofoil of four inches chord beneath the undisturbed free surface at velocities of 12 and 18 ft./sec. These agree with the trends of the theory but not with the magnitudes, the submergence always being greater than that predicted by the theory.

LIST OF SYMBOLS

b	Parameter defined in Eq. (4.1)
b'	Parameter defined in Eq. (4.3)
c	Parameter defined in Eq. (4.1)
C_h	Chord of the flat plate
C_L	Lift Coefficient
C_{L_a}	The slope of lift coefficient
d	Height of free surface above the leading edge shown in Fig. 4
D	Drag of the flat plate
e	Drop of lower cavity wall shown in Fig. 4
e'	Rise of free surface shown in Fig. 4
E	Complete elliptic integral of the second kind
$E(\varphi, k)$	Incomplete elliptic integral of the second kind
$F(\varphi, k)$	Incomplete elliptic integral of the first kind
g	Function defined in Eq. (3.4)
h	Height of the leading edge of the plate shown in Fig. 4
H	Depth of the flow at upstream infinity
I	Double integral defined in Eq. (4.25)
J	Integral defined in Eq. (4.12)
k	Modulus of the elliptic integrals, $k^2 = \frac{1}{b}$
k'	Complementary modulus of the elliptic integral
K	Complete elliptic integral of the first kind
ℓ	Length of the bottom wall shown in Fig. 1
L	Lift of the flat plate

M	Double integral defined in Eq. (4.24)
n	Image point of N on ζ-plane shown in Fig. 3.
N	Point on the free surface just above the leading edge of the plate shown in Fig. 4.
$\vec{q}$	Velocity vector
U	Velocity of the undisturbed stream
u, v	Perturbation velocity components in x and y directions respectively
$w(z)$	Complex perturbation velocity, $w = u - iv$
x, y	Cartesian coordinates
z	Complex variable of the physical plane in linearized version, $z = x + iy$
α	Angle of incidence of the plate
α^2	Parameter in the elliptic integral of the third kind
δ	Asymptotic spray sheet thickness
ζ	Complex variable of the transformed plane, $\zeta = \xi + i\eta$
θ	Inclination of the streamline
θ_1, θ_2	Asymptotic inclinations of the spray sheet and the free jet respectively
Λ_o	Lambda function
$\Pi(\alpha^2, k)$	Complete elliptic integral of the third kind
$\Pi(\varphi, \alpha^2, k)$	Incomplete elliptic integral of the third kind
ρ	Density of the water

1. Introduction

Recently, several papers dealing with the presence of a free surface in the proximity of a lifting, fully cavitating hydrofoil have appeared. Of these, one by Dawson and Bate[1] is primarily experimental. In their work a cavitating or ventilated flat plate hydrofoil was investigated near a free surface. The submergence was varied so that the hydrofoil went from a cavitating condition to a planing condition near the surface. Forces were measured in this experiment and compared to the results of several free-streamline theories applicable to this type of flow. One of these is a linearized theory for the flow of an infinitely deep stream past a cavitating hydrofoil in the presence of a free surface. This is the linearized theory due to Schot.[2] Johnson[3] considers both flat plate and cambered hydrofoils of finite aspect ratio near a free surface. This latter work is largely experimental. In these cases mentioned, both experiment and theory are concerned with hydrofoils at small angles of attack relatively near a free surface, i.e. two chords and less, and with small cavitation numbers approaching zero. Furthermore, the influence of gravity has been everywhere neglected. The most complete theory which has so far been produced, is an exact non-linear theory due to Green.[4] He considers in one of his papers the planing of a two-dimensional flat plate, without the influence of gravity, on a stream of finite depth. Although Green's work is

exact and the linear theories reported by Schot and referred to by Dawson and Bate are not, Green, however, did not compute a sufficient number of cases of interest to users of water tunnels. Furthermore, his solutions are not presented in an easily usable form. All free surface water tunnel experiments are conducted in a channel of finite depth, as opposed to the analyses of Refs. (2) and (3). The measurements of Dawson and Bate, particularly near the free surface, do not agree well with the calculations of the submergence effect to be found, for example, in Ref. (2), and it was suggested in Ref. (1) that the discrepancies are probably not due only to the influence of gravity, at least as estimated by current planing theories.[5] Briefly, the submergence effect on the lift of a flat plate hydrofoil is to increase the lift force as the surface is approached. In the limiting case of zero cavitation number, the cavity is, of course, infinitely long and the lift-slope goes from the value of $\pi/2$ for infinitely deep submergence to the value π at the surface for infinitesimal angles of attack. In the experiment of Ref. (1) the lift increases more slowly as the surface is approached than is indicated by linearized theory for flows of infinite depth and zero cavitation number. Incidentally, the lift-slopes are reasonably well accounted for by the theory. Until a complete solution accounting for all of the effects of non-zero cavitation number, channel depth and neighboring free surface is available, the exact cause of this discrepancy probably cannot be determined. In the present report, however, it has been decided to remove at least one of the drawbacks of the theoretical work mentioned previously; namely, there is a bottom at a finite distance beneath the hydro-

foil. Of course, Green's exact theory accounts for this effect. It was believed, however, that it was no more work to solve the problem anew by means of the linearized free streamline theory than to recalculate Green's exact solution. In fact, because of the flexibility afforded by the linear theory in determining the flow past relatively complex shapes and non-zero cavitation numbers, it was decided to follow this course rather than that of the exact theory. The linear theory, while suffering notable limitations is expected to provide a good value for the lift-slope at vanishing angles of attack and to account properly for the effects of submergence depth of channel, and even for the effect of a finite length of the bottom channel if such is the case.

The results of the calculations to be presented herein should be of some value to the users of water tunnels. Extensive tables and charts of the various force and geometric quantities involved are presented. In addition, the method of computing the results and the approximations for digital computations used herewith, are discussed in some detail* so that the reader may calculate additional cases for himself. In a subsequent report it is planned to consider the case of non-zero cavitation numbers.

2. Formulation of the problem

We shall apply the free streamline theory to the steady, two-dimensional flow past a flat plate. The stream is of finite depth with the upper surface bounded by a free surface, and the lower surface bounded partly by

---

* A companion report (Ref. (8)) may also be consulted for the computational method used.

a solid wall and partly by a free jet. The plate, which has both sharp leading and trailing edges, is inclined at a certain angle of incidence. A spray sheet is formed at the leading edge but the flow off the trailing edge is smooth. The sharpness of the edges allows one to expect that the separations of flow occur at these points as shown in Fig. 1. Far downstream, the spray sheet and the free jet become inclined at certain angles to the oncoming flow. The magnitude of the velocity along these surfaces equals that of the free stream.

Certain simplifications are then introduced into the problem:

i) the gravity effect is neglected throughout the analysis,

ii) the cavitation number is zero (infinitely long cavity),

iii) the angle of incidence of the plate with the free stream as well as the final inclinations of the spray sheet and jet are assumed to be small so that linearization of the problem is permitted.

If we denote the velocity by $\vec{q}$ then a complex perturbation velocity function

$$w(z) = u - iv \tag{2.1}$$

can be introduced such that $\vec{q} = U(1 + u, v)$.

The dimensionless perturbation velocity components $u(x, y)$ and $v(x, y)$ are assumed to be much smaller than unity. Applying the usual linearized boundary condition on the free surfaces, the plate and the solid wall, we have

$u = 0$ on all free surfaces (constant pressure and speed)

$v = -a$ on the wetted side of the flat plate,

$v = 0$ on the solid wall forming part of the lower boundary.

The linearized version of the above problem may then be depicted schematically in a complex z-plane as shown in Fig. 2.

One would notice that after linearization, the stagnation point on the plate coincides with the leading edge, furthermore, the streamline at that point splits into two branches.

In addition to the above boundary conditions, the perturbation velocity components must satisfy the following physical conditions:

i) there is a singularity at the leading edge,

ii) the streamline has a continuous slope at the plate-cavity juction (Kutta condition),

iii) the perturbation velocity components vanish upstream (at $x = -\infty$).

3. Preliminary results

We denote the depth of the stream at upstream infinity by H, the thickness of the spray sheet by δ, and the final inclinations of the spray and jet by θ_1 and θ_2 respectively. These quantities, essential in our calculations of the force coefficient and the flow geometry, are to be determined from the theory. In addition, the following quantities are specified: U the velocity of the free stream, C_h the length of the plate, α the angle of incidence, h the height of the plate leading edge above the bottom

wall, and ℓ the length of the bottom solid wall downstream of the leading edge. The submergence of the hydrofoil beneath the undisturbed oncoming flow is the difference between H and h, i.e., H – h. We shall now make a preliminary calculation based on continuity and momentum considerations which gives some useful relations between the forces and flow geometry.

The ultimate thickness of the spray sheet and lower jet must equal the upstream depth by the continuity relation. Thus if $\epsilon = \delta/H$, the thickness of the jet is $(1 - \epsilon)H$. The drag on the plate can be found from a momentum balance and in terms of ϵ it is

$$D = \frac{\rho U^2 H}{2}\left[\epsilon\theta_1^2 + (1-\epsilon)\theta_2^2\right] \tag{3.1}$$

using the approximation $\cos\theta = 1 - \theta^2/2$ etc. When the hydrofoil is a flat plate the force on the plate must be normal to the surface. Thus, if L and D are the lift and drag force perpendicular to and parallel to respectively the oncoming flow of speed U,

$$D = L\tan\alpha \tilde{=} L\alpha \tag{3.2}$$

where α, assumed small, is the angle of attack of the plate with respect to the oncoming flow.

The lift coefficient is defined as

$$C_L = \frac{L}{\frac{1}{2}\rho U^2 C_h}$$

hence

$$C_L = \frac{\delta}{C_h\alpha}\left[\theta_1^2 + \frac{(1-\epsilon)}{\epsilon}\theta_2^2\right] \tag{3.3}$$

Given the depth above the bottom, h, and the upstream depth, H, we may expect that the spray sheet thickness, δ, and hence ϵ will vary with angle of attack. We anticipate that in the linear theory already sketched in section (2), velocities and hence angles such as θ_1, etc. are proportional to α. the angle of attack. Thus

$$C_L = \frac{\delta \alpha}{C_h}\left[\left(\frac{\theta_1}{\alpha}\right)^2 + \frac{1-\epsilon}{\epsilon}\left(\frac{\theta_2}{\alpha}\right)^2\right]$$

and the ratios θ_1/α etc., will be independent of α in the present theory. But δ, within our linear theory, can contain a linear term in α. Now in the limit as α approaches zero, the spray sheet thickness will approach d. Thus we can put

$$\delta = d - \alpha g \tag{3.4}$$

where g is a function only of the geometrical ratios C_h/d, C_h/h which has to be determined from the theory. For vanishingly small angles of attack we will have

$$\frac{dC_L}{d\alpha} \equiv C_{L_\alpha} = \frac{d}{C_h}\left[\left(\frac{\theta_1}{\alpha}\right)^2 + \frac{h}{d}\left(\frac{\theta_2}{\alpha}\right)^2\right] \tag{3.5}$$

and for larger angles (restricting ourselves now to the case of a rigid, flat bottom for which θ_2 is zero) we have

$$C_{L_\alpha} = \left[\frac{d}{C_h} - \frac{2\alpha g}{C_h}\right]\left(\frac{\theta_1}{\alpha}\right)^2 \tag{3.6}$$

We will now develop the linear theory to determine the quantities (θ_1/α), (θ_2/α), and g. With these and given values of d, h, and C_h the spray sheet thickness, submergence and lift of the hydrofoil can be determined.

4. Theory

Consider the transformation

$$z = -b \log\left(1 + \frac{\zeta}{b}\right) - c \log\left(1 - \frac{\zeta}{c}\right) \qquad (4.1)$$

where $\zeta = \xi + i\eta$.

The flow in the physical plane is mapped into the upper half ζ-plane and the entire boundary of the flow goes into the real axis, shown in Fig. 3. The leading and trailing edges of the plate in the z-plane are at the origin and -1 respectively. Upstream infinity, A, transforms into infinity. The end of the solid wall, B', the free jet, B, and the spray sheet, C, have their corresponding image points at $-b'$, b and c. The value of b approaches b' as the length ℓ is extended to infinity. The quantities b', b and c are parameters whose numerical values will be determined later from the mapping function. We know, however, at this stage $c > 0$, $b' \geq b > 1$.

The complex perturbation velocity in ζ-plane, denoted by

$$\nu(\zeta) = u - iv$$

takes the following boundary values on the $R\ell\ \zeta$ or ξ axis.

$$\begin{aligned} v &= 0 && -\infty < \xi < -b' \\ u &= 0 && -b' < \xi < -1 \\ v &= -a && -1 < \xi < 0 \\ u &= 0 && 0 < \xi < \infty . \end{aligned}$$

The flow in the upper half ζ-plane can be continued analytically into the lower half by

$$\nu(\bar{\zeta}) = -\overline{\nu(\zeta)} . \qquad (4.2)$$

On the $R\ell\ \zeta$ axis, two branch cuts appear; one starts from $\xi = -\infty$ to $-b'$ and the other from $\xi = -1$ to the origin. These cuts correspond

to the plate and the solid wall in the physical plane respectively. We now have a boundary value problem involving the unknown function $\nu(\zeta)$ which can be formulated and solved as a Hilbert problem.[6]

We introduce the auxiliary function

$$H(\zeta) = i\sqrt{\frac{\zeta}{(\zeta+1)(\zeta+b')}}, \tag{4.3}$$

which as the following properties

i) $H(\zeta)$ has the proper branch cuts ($\zeta = 0, -1, -b'$ and ∞ are branch points).

ii) It provides the correct leading edge singularity (square root singulaity).

iii) On the $R\ell\,\zeta$ axis;

$$\begin{aligned}
&\mathrm{Im}\,H = 0 && -\infty < \xi < -b' \\
&R\ell\,H = 0 && -b' < \xi < -1 \\
&R\ell\,H = -\sqrt{\frac{-\xi}{(1+\xi)(b'+\xi)}}, \quad \mathrm{Im}\,H = 0 && -1 < \xi < 0 \\
&R\ell\,H = 0 && 0 < \xi .
\end{aligned}$$

A new function

$$G(\zeta) = \nu(\zeta)\,H(\zeta) \tag{4.4}$$

is then formed which has on the $R\ell\,\zeta$ axis;

$$\begin{aligned}
&\mathrm{Im}\,G = 0 && -\infty < \xi < -b' \\
&\mathrm{Im}\,G = 0 && -b' < \xi < -1 \\
&\mathrm{Im}\,G = -a\sqrt{\frac{-\xi}{(1+\xi)(b'+\xi)}} && -1 < \xi < 0 \\
&\mathrm{Im}\,G = 0 && 0 < \xi .
\end{aligned}$$

With the aid of Plemelj's formula.[6] the solution of the Hilbert

problem is given immediately by*

$$\nu(\zeta) = u - iv = -\frac{ia}{\pi}\sqrt{\frac{(\zeta+1)(\zeta+b')}{\zeta}}\int_{-1}^{0}\sqrt{\frac{-t}{(1+t)(b'+t)}}\ \frac{dt}{\zeta-t}\ . \tag{4.5}$$

In order to evaluate the final inclinations θ_1 and θ_2 we notice that according to the linearized theory, the streamline has a slope

$$\frac{dy}{dx} = \theta = v\ . \tag{4.6}$$

In addition, the boundary conditions on the free surface require that everywhere $u = 0$. Hence, we obtain

$$\theta_1 = -\mathrm{Im}\,\nu(c) = \frac{a}{\pi}\sqrt{\frac{(c+1)(c+b')}{c}}\int_{-1}^{0}\sqrt{\frac{-t}{(1+t)(b'+t)}}\ \frac{dt}{c-t}\ , \tag{4.7}$$

and

$$\theta_2 = -\mathrm{Im}\,\nu(-b) = -\frac{a}{\pi}\sqrt{\frac{(b-1)(b'-b)}{b}}\int_{-1}^{0}\frac{1}{b'+t}\sqrt{\frac{-t}{(1+t)(b'+t)}}\,dt\ . \tag{4.8}$$

The mapping function gives us the following relations of the desired parameters.

$$C_h = -b\log\left(1-\frac{1}{b}\right) - c\log\left(1+\frac{1}{c}\right)\ , \tag{4.9}$$

$$B' = -b\log\left(1+\frac{b'}{b}\right) - c\log\left(1-\frac{b'}{c}\right)\ , \tag{4.10}$$

where $B' = \ell - i\pi h$,

and $h = \pi b$. (4.11)

By specifying the ratio C_h/h and the length of the wall ℓ, values of b', b and c can be calculated from these simultaneous equations. The detailed evaluation of these quantities will be given in a later part of the report.

The geometry of the problem can also be solved since the velocity

---

* No complimentary function is needed here and Eq. (4.5) is the complete solution.

field is now known. To simplify the matter, the limiting case of an infinitely long solid wall will be worked out (for which $b \to b'$). The reader may refer all quantities in the following calculation to Fig. 4.

Denote
$$J = \int_{-1}^{0} \frac{dt}{t-c} \sqrt{\frac{-t}{(1+t)(b+t)}} \quad , \tag{4.12}$$

thus
$$\theta_1 = -\frac{a}{\pi} \sqrt{\frac{(c+1)(b+c)}{c}}\, J \quad , \tag{4.13}$$

$$\theta_2 = 0 \tag{4.14}$$

and
$$C_{L_a} = \frac{\delta}{C_h} \frac{(c+1)(c+b)}{c}\, J^2 \tag{4.15}$$

Since $b > 1$ and $c > 0$ at all times we may introduce new parameters k and k' such that

$$k^2 = \frac{1}{b} < 1$$

and
$$k'^2 = 1 - k^2 < 1$$

The integral J can now be written in terms of known eliptic functions[7] in the form

$$J = 2k\left[\Pi\left(-\frac{1}{c}, k\right) - K\right] \tag{4.16a}$$

or in an alternate form

$$J = \pi \sqrt{\frac{c}{(1+c)(b+c)}}\, \Lambda_o(\psi, k) - \frac{2\sqrt{b}}{b+c}\, K \tag{4.16b}$$

where

$$\Lambda_o(\psi, k) = \frac{2}{\pi}\left[EF(\psi, k') + KE(\psi, k') - KF(\psi, k')\right]$$

is Heuman's Lambda function, K and E are the complete elliptic integrals of the first and second kind of modulus k, and $F(\psi, k')$ and $E(\psi, k')$ are the incomplete elliptic integrals of the second kind of amplitude ψ, and

modulus (complementary) k'.

The next quantities that we wish to determine are the submergence, $H-h$, and the spray sheet thickness, δ. With reference again to Fig. 4, one may derive the submergence by combining the continuity equation and geometry of the flow, i.e.,

$$H - h = d - e', \tag{4.17}$$

where e' is the rise in free surface from upstream infinity to the point N at the distance d above the leading edge of the plate. The same relations give the spray sheet thickness.

$$\delta = d - (e' - e - C_h a), \tag{4.18}$$

where e is the drop along the lower cavity wall from the trailing edge to downstream infinity. Comparing the above expression for δ to our definition of g given in Eq. (3.4), one may immediately write

$$g = \frac{1}{a}(e' - e) - C_h . \tag{4.19}$$

We shall apply our present theory to determine e and e'.

In linearized theory, it is known that the vertical difference between two points on the same streamline can be calculated by considering an integral, in the physical plane, of the form

$$\int v \, dx,$$

where values of v are taken along horizontal lines which approximate the actual streamline. In our problem, all free surfaces in the physical plane are mapped onto the real axis of the ζ-plane. The above integral can then be replaced by an equivalent one,

$$\int \nu(\zeta) \frac{dz}{d\zeta} \, d\zeta ,$$

carried along the real ζ-axis. This enables us to write with reference to Fig. 3,

$$e' = \int_n^{\infty} \nu(\zeta) \frac{dz}{d\zeta} \, d\zeta \, , \tag{4.20}$$

and

$$e = \int_{-1}^{b} \nu(\zeta) \frac{dz}{d\zeta} \, d\zeta \, . \tag{4.21}$$

The lower limit, n, in Eq. (4.20) is the image of N in the z-plane and has to be determined by solving a transcendental equation. Finally, with the aid of the mapping function in Eq. (4.1) one may write

$$e' = \frac{a}{\pi} M, \tag{4.22}$$

where M is the double integral

$$M = \int_n^{\infty} \left[\frac{b}{b+\xi} + \frac{c}{\xi - c} \right] \sqrt{\frac{(\xi+1)(\xi+b)}{\xi}} \int_{-1}^{0} \frac{dt}{\xi - t} \sqrt{\frac{-t}{(1+t)(b+t)}} \, d\xi \, , \tag{4.23}$$

and

$$e = \frac{a}{\pi} I \, , \tag{4.24}$$

where I is the double integral

$$I = \int_{-1}^{-b} \left[\frac{b}{b+\xi} + \frac{c}{\xi - c} \right] \sqrt{\frac{(\xi+1)(\xi+b)}{\xi}} \int_{-1}^{0} \frac{dt}{\xi - t} \sqrt{\frac{-t}{(1+t)(b+t)}} \, d\xi . \tag{4.25}$$

All that now remains is to determine n and to evaluate the double integrals M and I.

i) The number n:

For the calculation of n, one has to utilize the mapping function in Eq. (4.1). Since N is purely imaginary and n real, the substitution of N for z and n for ζ into Eq. (4.1) gives

$$b \log \frac{n+b}{b} + c \log \frac{n-c}{c} = 0 \, ,$$

or $$(n/b + 1)^b \ (n/c - 1)^c = 1 \qquad (4.26)$$

Equation (4.26) is a transcendental one, such that for given values of b and c, n must be determined by iteration. One knows, however, that n lies in the interval bounded by c and 2c.

ii) The double integral M:

The inner integral in Eq. (4.23) can also be expressed in terms of complete elliptic integrals of the first and third kind. If we further replace the integration variable ξ by $1/s$, M can now be written as a single integral,

$$M = 2K \int_0^{\frac{1}{n}} \left[\frac{1}{s+k^2} + \frac{c}{1-cs} \right] \sqrt{\frac{s+1}{s(s+k^2)}}\, ds - \pi \int_0^{\frac{1}{n}} \left[\frac{1}{s+k^2} + \frac{c}{1-cs} \right] \frac{\Lambda_o(\Psi, k)}{s}\, ds \,, \qquad (4.27)$$

where $\Psi = \sin^{-1} \sqrt{\frac{s}{s+k^2}}$.

The first integral in Eq. (4.27) can easily be reduced to incomplete elliptic integrals and M now can be expressed as

$$M = 4K \left[\frac{E(\varphi_1, k')}{k^2} + \frac{ck^2(1+c)}{ck^2+1} \Pi(\varphi_1, \alpha_1^2, k') + \frac{ck'^2}{1+ck^2} F(\varphi_1, k') \right]$$
$$- \pi \int_0^{\frac{1}{n}} \left[\frac{1}{s+k^2} + \frac{c}{1-cs} \right] \frac{\Lambda_o(\Psi, k)}{s}\, ds \qquad (4.28)$$

where $\varphi_1 = \sin^{-1} \sqrt{\frac{1}{1+nk^2}} < \frac{\pi}{2}$, and $\alpha_1^2 = 1 + ck^2 > 1$.

The remaining integral will be treated numerically. For this purpose one must examine the behavior of Λ_o/s for small s. By definition,

$$\Lambda_o(\Psi, k) = \frac{2}{\pi} \left[(E-K)F(\Psi, k') + KE(\Psi, k') \right] .$$

For any non-zero k, Ψ approaches zero as s approaches zero. One may therefore apply binomial expansions to the integrands of $F(\Psi, k')$ and $E(\Psi, k')$ and integrate term by term. By so doing the asymptotic behavior of $\Lambda_o(\Psi, k)$ as Ψ approaches zero is found to be

$$\Lambda_o(\Psi, k) \sim \frac{2}{\pi} E \Psi + 0(\Psi^3) . \tag{4.29}$$

A second expansion of Ψ is then carried out to yield, for small values of s,

$$\Psi \sim \left(\frac{s}{s+k^2}\right)^{\frac{1}{2}} + O\left[\left(\frac{s}{s+k^2}\right)\right]^{\frac{3}{2}} \tag{4.30}$$

Hence, by keeping only the first term,

$$\frac{\Lambda_o(\Psi, k)}{s} \sim \frac{2}{\pi} \frac{E}{\sqrt{s(s+k^2)}} . \tag{4.31}$$

We have therefore found that the term Λ_o/s is singular at $s = 0$, however, the singularity is of the order of one half, and is thus integrable. In order to facilitate numerical computation, we regroup the integrand in the following form;

$$\begin{aligned} & -\pi \int_0^{\frac{1}{n}} \left[\frac{1}{s+k^2} + \frac{c}{1-cs}\right] \frac{\Lambda_o(\Psi, k)}{s} \, ds \\ & = \int_0^{\frac{1}{n}} \left[\frac{1}{s+k^2} + \frac{c}{1-cs}\right] \left[\frac{2E}{\sqrt{s(s+k^2)}} - \pi \frac{\Lambda_o(\Psi, k)}{s}\right] ds \\ & - 2E \int_0^{\frac{1}{n}} \left[\frac{1}{s+k^2} + \frac{c}{1-cs}\right] \frac{ds}{\sqrt{s(s+k^2)}} . \end{aligned} \tag{4.32}$$

The singular behavior of the integrand is thereby subtracted out, so that the first integral presents no difficulty in computation and the second integral can be integrated in closed form.

Summarizing the results for M-integral, we have

$$M = 4K\left[\frac{E(\varphi_1, k')}{k^2} + \frac{ck^2(1+c)}{ck^2+1}\Pi(\varphi_1, a_1^2, k') + \frac{ck^2}{1+ck^2}F(\varphi_1, k')\right]$$

$$-\frac{4E}{k^2}\left\{\frac{1}{\sqrt{1+nk^2}} - \frac{1}{\sqrt{a^2-1}}\left[\log\frac{e^{2\theta_o}-t_1}{e^{2\theta_o}-t_2} - \log\left|\frac{1-t_1}{1-t_2}\right|\right]\right\}$$

$$+\int_o^1\left[\frac{1}{s+k^2} + \frac{c}{1-cs}\right]\left[\frac{2E}{\sqrt{s(s+k^2)}} - \pi\frac{\Lambda_o(\Psi,k)}{s}\right]ds\,. \qquad (4.33)$$

where $a = 1 + \frac{2}{ck^2}$, $\theta_o = \sinh^{-1}\sqrt{\frac{1}{nk^2}}$, $t_1 = a + \sqrt{a^2-1}$

and $t_2 = a - \sqrt{a^2-1}$.

iii) The double integral I:

The treatment of the integral I is quite similar to that of M. First, the inner integral is expressed in terms of complete elliptic integrals to reduce I to the single integral,

$$I = \pi\int_1^b\left[\frac{b}{b-\xi} - \frac{c}{c+\xi}\right]\left[1 - \Lambda_o(\beta,k)\right]d\xi\,, \qquad (4.34)$$

where $\beta = \sin^{-1}\sqrt{\frac{\xi-1}{\xi}\,\frac{b}{b-1}}$, $0 \le \beta \le \frac{\pi}{2}$.

The whole I integral will be treated numerically. As in treating the M integral, we shall examine first the behavior of the quantity $(1-\Lambda_o)/(b-\xi)$ near $\xi = b$. With the aid of Legendre's relation, i.e.,

$$EK' + E'k - KK' = \frac{\pi}{2}\,,$$

the term, $1 - \Lambda_o(\beta, k)$ vanishes as β approaches $\frac{\pi}{2}$, or when ξ approaches b. One can show further that in the neighborhood of b, $1 - \Lambda_o$

behaves like the square root of the quantity $b - \xi$, or more precisely,

$$1 - \Lambda_o(\beta, k) \sim \frac{2k}{\pi} \left[\frac{E}{k'} - Kk' \right] \sqrt{b-\xi} \tag{4.35}$$

We therefore apply the same technique as we did in the treatment of M integral to yield.

$$I = I_1 + I_2 \tag{4.36}$$

where

$$I_1 = \pi \int_1^b \frac{b}{b-\xi} \left[1 - \Lambda_o(\beta, k) \right] d\xi$$

$$= \pi \int_1^b \frac{b}{b-\xi} \left\{ \left[1 - \Lambda_o(\beta, k) \right] - \frac{2k}{\pi} \left[\frac{E}{k'} - Kk' \right] \sqrt{b-\xi} \right\} d\xi$$

$$+ 4k' \left[\frac{E}{k'} - Kk' \right] , \tag{4.36a}$$

and

$$I_2 = -\pi c \int_1^b \frac{1}{c+\xi} \left[1 - \Lambda_o(\beta, k) \right] d\xi . \tag{4.36b}$$

The numerical computations are described in detail in the appendix. All numerical integrations are carried out on the IBM 7090 computer at the computing center at the California Institute of Technology.

5. Limiting cases

The present solution contains several geometrical parameters such as h, ℓ, etc. When these parameters approach zero or infinity several interesting but simpler flows are obtained. Recovery of results for simple flows from solutions of a more general one often serves as an indication of the correctness of the general solution and also provides one certain useful information about the behavior of the solution near such limits. We shall consider several cases. The parameters to be varied are the dis-

tances h and d, and the ratios C_h/d and C_h/h. In all cases, we are interested in the behavior of the slope of the lift coefficient C_{L_α}. The length of the wall l is equal to positive infinity, i. e. a completely rigid bottom for the first four cases and negative infinity (or a free jet) for the last one.

All cases are for vanishing angle of attack so that we may put $\delta = d$.

Case 1: The infinitely deep stream ($h \to \infty$).

Given a plate of finite length C_h, the limit $C_h/h \to 0$ implies that h or b approach infinity, or that the stream becomes infinitely deep. C_{L_α} as a function of C_h/d is then given by the simultaneous equations

$$C_h/d = \frac{1}{d} - \frac{1}{\pi} \log (1 + \pi/d)$$

$$C_{L_\alpha} = \frac{1}{C_h/d} \left(1 + \frac{\pi}{d}\right) \left[1 - \left(1 + \frac{\pi}{d}\right)^{-\frac{1}{2}}\right]^2$$

as may be found from Eqs. (4. 9) and (4. 15). These results agree with those of Schot[2]. Again it should be noticed that as the submergence approaches zero, C_L tends to the limit π, and for the infinite fluid case, C_L approaches $\pi/2$.

Case 2: Planing on a stream of finite depth ($d \to 0$).

Since d, the spray sheet thickness, vanishes, this case corresponds to that of planing. We obtain for this limit

$$C_{L_\alpha} = \frac{4}{C_h \pi} K^2$$

near $d = 0$. Introducing a new parameter k_1, such that

$$k_1 = \frac{1 - k'}{1 + k'}$$

Reference (7) gives the following expansion of K

$$K = \frac{\pi}{2}(1 + k_1)\ F\left(\frac{1}{2}, \frac{1}{2}; 1, k_1^2\right)$$

where F is the usual hypergeometric function.

Now we let the depth of the stream become large and the leading terms of the following expansions are readily obtained:

$$k_1 = \frac{1}{4b}\left(1 - \frac{1}{2b}\right) + 0\left(\frac{1}{b^3}\right),$$

$$K^2 = \left(\frac{\pi}{2}\right)^2\left[1 + \frac{1}{2b} + \frac{11}{32}\ \frac{1}{b^2} + 0\left(\frac{1}{b^3}\right)\right],$$

and

$$C_{L_a} = \frac{\pi}{C_h}\left[1 + \frac{1}{2b} + \frac{11}{32}\ \frac{1}{b^2} + 0\left(\frac{1}{b^3}\right)\right].$$

From the mapping relation, we have

$$\frac{\pi C_h}{h} = \frac{1}{b}\left(1 + \frac{1}{2b}\right) + 0\left(\frac{1}{b^3}\right)$$

and if the above relations are combined for small ratios of C_h/h, we have the approximate result

$$C_{L_a} = \pi\left[1 + 0.102808\ (C_h/h)^2\right].$$

The first term is the result of planing with infinite depth at infinite Froude number.[5] The total expression for C_{L_a} ignoring terms less than b^{-2} is very close to the result of Dawson[1] which gives

$$C_{L_a} = \left[1 + 0.103\ (C_h/h)^2\right].$$

Case 3: Flow past a cavitating plate near a solid wall ($d \to \infty$).

This limit corresponds to the case of infinite submergence. The plate, however, is held at an arbitrary distance from the wall. C_{L_a} as a function of the distance h (or b) is now governed by the simultaneous equations

$$C_{L_a} = \frac{4b}{C_h \pi} (K - E)^2$$

and

$$C_h = -\frac{1}{b} \log \left(1 - \frac{1}{b}\right) - 1.$$

We will now obtain the first order wall effect by letting h become large. We obtain after a little manipulation the approximate result

$$C_{L_a} = \frac{\pi}{2} \left[1 + 0.208 \sqrt{C_h/h} \right]$$

The constant term again is a well known result of infinite fluid flow.

Case 4: The case of very large chord ($C_h \to \infty$).

There are two simple limiting situations: One of zero submergence and one of infinite submergence. We will consider them separately.

i) Zero submergence. We may set c in the mapping function to be zero to obtain

$$\exp \left[-\frac{\pi C_h}{h} \right] = 1 - \frac{1}{h} = k'^2.$$

The slope of lift coefficient now becomes

$$C_{L_a} = \frac{4}{C_h \pi} K^2$$

for this case. Now we will let the chord become large compared to the depth, so that C_h/h approaches infinity and k' approaches zero. The K function has then the well known behavior

$$K \to \log 4/k'.$$

If we substitute log 4/k', for K into C_{L_a}, we have

$$\lim_{C_h/h \to \infty} \frac{C_{L_a}}{C_h/h} = 1.$$

or C_{L_a} grows linearly in C_h/h when C_h/h is large.

This result is almost intuitively apparent since the plate is then subject to stagnation pressure over the whole surface.

ii) Infinite submergence.

The mapping yields the relation

$$-\pi \frac{C_h}{h} = \frac{\pi}{h} + \log\left(1 - \frac{1}{b}\right),$$

and the lift slope

$$C_{L_a} = \frac{4b}{C_h \pi} (K - E)^2.$$

As $b \to 1$,

$$C_{L_a} = \frac{4}{\pi^2} \frac{1}{C_h \pi} \left[(\log 4 - 1) - \frac{1}{2} \left(1 + \frac{\pi C_h}{h} \right) \right]^2$$

and

$$\lim_{C_h/h \to \infty} \frac{C_{L_a}}{C_h/h} = 1.$$

We get the same result as the previous case.

Case 5: The free jet ($\ell = -\infty$).

The entire flow in this case becomes a free jet. The parameter b' in Eq. (4.10) approaches plus infinity as the bottom wall vanishes, and the asymptotic angles of inclination, θ_1 and θ_2 given in Eqs (4.7) and (4.8), can be integrated in closed form to give the following result for C_{L_a} with the use of Eq. (3.5)

$$C_{L_\alpha} = \frac{\pi c}{C_h}\left[\left(\sqrt{1+\frac{1}{c}}-1\right)^2 + \frac{h}{\pi c}\left(1-\sqrt{1-\frac{1}{b}}\right)^2\right] .$$

This result and that of mapping function (Eq. 4. 9) give the complete solution for the cavitating flow past a flat plate hydrofoil in a free jet. As a further special case to illustrate the effect of a lower free jet let us take the submergence to be infinite. Then, c approaches infinity and the mapping function Eq. (4. 9) becomes

$$C_h/h = -\frac{1}{\pi}\log\left(1-\frac{1}{b}\right) - \frac{1}{\pi b} .$$

When the hydrofoil approaches the bottom closely, b approaches unity and the following approximate formula for C_{L_α} can be quickly established

$$C_{L_\alpha} = \frac{h}{C_h}\left\{1 - \exp\left[-\frac{\pi}{2}\left(\frac{C_h}{h}+\frac{1}{\pi}\right)\right]\right\}^2$$

valid for large values of C_h/h. Thus, the lift slope vanishes when the hydrofoil is on the lower free surface and grows linearly with depth for small submergences.

6. Numerical Results

The majority of the numerical results presented herein are for the case of the infinitely long bottom wall. To bring out the salient features of this more common situation, we have chosen several values of C_h/h, within the usual range of experimental interest, and calculated the lift slope, C_{L_α}, the spray sheet contraction, δ/d, as functions of the chord spray-sheet thickness ratio, C_h/d, and the dimensionless submergence ratio, $(H-h)/C_h$. These are shown in Figs. 5, 6 and 7 respectively.

An inspection of Fig. 5 brings out the fact that the effect of the bottom and that of the free surface are in the same direction; namely, to increase the lift slope. Moreover, the influence of both the bottom and the free surface extends to many chords and decreases even then at a slow rate. For example, the fully submerged limit ($C_{L_\alpha} = \pi/2$) is not reached even with a submergence of 100 chords; and the presence of the bottom is still in evidence with ten chords of depth beneath the foil.

Interestingly, the spray sheet contraction δ/d shows only a minor dependence on channel depth ratio, C_h/h, but it is affected to a marked degree by the angle of attack. This is, of course, just the effect of g as indicated in Eq. (3.4). In fact, it would have been perhaps more illustrative to plot the ratio of g/d rather than that of δ/d as is done in Fig. 6. In any event, even at the moderate angle of six degrees, the spray sheet can become significantly less than distance d. We may add that previous linearized theories have not distinguished between these quantities.

The submergence of the hydrofoil beneath the undisturbed surface is given in Fig. 7 for various ratios of C_h/d and chord-depth ratio C_h/h. The submergence, like the spray sheet will depend upon the angle of attack. At vanishingly small angles, the submergence becomes equal to the quantity d, but even at small angles it is seen to become appreciably less than this. The submergence ratios in Fig. 7 are calculated for $\alpha = 6^o$. The limiting case $\alpha = 0$ is also shown. It is not surprising that for small values of C_h/h and large values of C_h/d that the submergence can become negative even leading to the

situation in which the entire hydrofoil lies above the undisturbed water level. This result is well-known from the previously mentioned work of Green.

For the finite-length bottom calculations, we chose the case where the plate is in midstream, that is $b = c$, and $C_h/h = 0.4$, because this situation corresponds to the usual experimental conditions in the Free Surface Water Tunnel at C.I.T. Figure 8 shows C_{L_α} versus ℓ/C_h for this case. When the bottom extends to approximately six chords downstream from the leading edge of the flat plate the free jet effect becomes negligible, so that the lift slope is essentially the same as that calculated for the infinite bottom case. Similarly, at approximately six chords upstream the lift slope approaches that of the completely free jet. This result shows that the length of bottom required to establish the infinite bottom effect is in reality only a few chords - say about three downstream of the hydrofoil. Interestingly, nearly the infinite fluid case is achieved when the bottom stops just underneath the leading edge of the hydrofoil. Seemingly, the free-surface effect and the bottom effect are then just about cancelled out.

The details of the present calculations are discussed in the Appendix and the intermediate parameters needed for the calculations and for calculations at other angles of attack than given so far are tabulated in Tables 1 and 2. The geometrical parameters b and c and the dependence of J on the quantities are graphed in Fig. A-1 of the Appendix.

7. Discussion

It would be desirable to be able to present experimental data confirming the theory just outlined. The ubiquitous presence of gravity, however, makes all such hopes faint; zero cavitation number--resulting in physically unrealistic infinite jets--is not possible in a gravitational environment. The indicated lift-slope values of Fig. 5 for geometries similar to those used by Dawson and Bate are far higher than those extrapolated from their experiments which were conducted at non-zero cavitation numbers. Undoubtedly the effects of the free surface and the rigid bottom are greatly augmented for zero cavitation number; in fully wetted flow, a relatively slight effect on C_{L_α} for the geometry of Fig. 8 would be expected, for example. Nearer the free surface it becomes possible to approach more closely the conditions of zero cavitation number so that the conditions of the theory will be more accurately met there.

To investigate this point a flat plate hydrofoil was mounted in a two-dimensional, parallel wall insert six inches wide in the Free Surface Water Tunnel similar in type to the one used by Dawson and Bate. Two photographs of the hydrofoil and resulting spray sheet are shown in Fig. 9. In these photographs three water surfaces can be seen: the level exterior to the two-dimensional insert, the lower and upper boundaries of the cavity, and finally the top of the spray sheet itself. The curving, exterior water surface just above the hydrofoil should be disregarded. It should be mentioned that the effects of friction on the inside of the channel result in a very gradual curvilinear flow, the surface of which is slightly inclined to the horizontal. Angles of attack were determined relative to this undisturb-

ed flow. It was not possible, however, to make sufficiently precise measurements of the effective angles of attack to permit C_{L_α} to be calculated. Measurements of the distance d and submergence below the undisturbed surface were, however, made and these are given in Fig. 10 for several angles of attack. Also shown are the theoretical values for the indicated angles, calculated for the geometry of the experiment. Data were taken at two speeds, 12 ft./sec. and 18 ft./sec. The chord of the hydrofoil was four inches.

It is apparent from Fig. 10 that the observed submergence is always greater than that calculated, and that the discrepancy increases with angle of attack. There is no perceptible difference in behavior with velocity (or Froude number) although one may observe in Fig. 9 that there is a substantial gravity effect on the spray sheet causing it to follow a curved trajectory. The actual magnitude of the difference in the observed and calculated value at 6° angle of attack amounts to about 0.1 chord or in the case of the present experiment nearly 0.4 inches. This is too large for experimental error. In these spray sheet measurements the cavity was vented to atmosphere. Nevertheless, there was still a hydrostatic gradient.

We are at somewhat of a loss for a quantitative explanation of the lack of agreement between the theory and experiment insofar as the spray sheet measurements go. The experiments do, however, follow the predicted trends, even exhibiting the negative submergence although to a smaller magnitude. Gravity would have such an effect as it tends to prevent the free surface from rising. At the same time, the observations suffer because the measurements were made in a rather narrow channel

(six inches). The sidewall boundary layers in the channel at the site of the hydrofoil amounted to about one-half inch in thickness[9] and there was also a small but undetermined curvature of the undisturbed free surface. The slope of this surface at the point of hydrofoil immersion was three degrees. With this combination of circumstances, one should, perhaps, not expect better agreement with a linear theory at zero cavitation number.

In closing, it is worthwhile to mention that it is easy to extend the present calculations to account for arbitrary hydrofoil shape. Furthermore, it is not much harder to carry the problem through for non-zero cavitation numbers provided one of the simpler "wake" models is adopted as the prescription for the flow.

ACKNOWLEDGMENTS

The authors wish to thank Miss Cecilia Lin for the illustrations, Mrs. Mary Goodwin for typing the manuscript and Mr. Ted Bate for carry-out the experimental work.

REFERENCES

1. Dawson, Thomas E. and Bate, E. R., Jr., "An Experimental Investigation of a Fully Cavitating Two-Dimensional Flat Plate Hydrofoil Near a Free Surface," California Institute of Technology, Hydrodynamics Laboratory, Report No. E-118.12, October 1962.

2. Schot, Steven H., "Surface Tension and Free Surface Effects in Steady Two-Dimensional Cavity Flow About Slender Bodies," David Taylor Model Basin, Report No. 1566, January 1962.

3. Johnson, Virgil E., Jr., "Theoretical and Experimental Investigation of Arbitrary Aspect Ratio, Supercavitating Hydrofoils Operating Near the Free Surface," NACA RM L57116, December 1957.

4. Green, A. E.,
(a) "Note on the Gliding of a Plate on the Surface of a Stream," Proceedings of Cambridge Philosophical Society, Vol. 32, 1936, pp. 248-252.

(b) "The Gliding of a Plate on a Stream of Finite Depth," Proceedings of Cambridge Philosophical Society, Part I, Vol. 31, 1935, pp. 584-603, Part II, Vol. 32, 1936, pp. 67-85.

5. Cumberbatch, E., "Two-Dimensional Planing at High Froude Number," Journal of Fluid Mechanics, Vol. 4, Part 5, September 1958, pp. 466-478.

6. Mikhlin, S. G., "Integral Equations," Pergamon Press, 1957

7. Byrd, Paul F. and Friedman, Morris D., "Handbook of Elliptic Integrals for Engineers and Physicists," Springer Verlag, 1954.

8. Ai, Daniel K. and Harrison, Z. L., "A Computer Method for Calculation of the Complete and Incomplete Elliptic Integrals of the Third Kind," California Institute of Technology, Hydrodynamics Laboratory, Report No. E-110.3, February 1964

9 Bate, E. R., Jr., "A Preliminary Study of Strut Interference and Wall Gap Effects on the Lift of a Supercavitating Flat Plate," California Institute of Technology, Hydrodynamics Laboratory, Internal Memorandum E-118.18.1M, March 1964.

APPENDIX: CALCULATION PROCEDURES

A. Infinitely Long Bottom Wall

The first step in the calculation of the desired quantities C_{L_a} $(H-h)/C_h$, δ/d, and C_h/d is to determine values of b and c for each specified C_h/h. This entails solving by iteration the transcendental equation given in Eq. (4.9). We should point out that once a value of C_h/h is prescribed, the values of b lie within a particular range and no solution outside that range is possible. The solid lines in Fig. A-1 are curves of constant C_h/h in the b-c plane. Notice that as C_h/h approaches unity, the range of b for which a solution exists becomes very narrow. These curves may be used, along with additional values given in Table 1, to obtain first approximations of b and c for values of C_h/h not tabulated.

Once a set of b's and c's are established, for the infinitely long bottom wall case, it is now easy to solve Eq. (4.16a) or (4.16b) for J and then obtain C_{L_a} from Eq. (4.15). If J is calculated on a high speed computer, Eq. (4.16a) is a convenient form to use as a computer method for evaluating $\Pi(\alpha^2, k)$ is given in Ref. (8). On the other hand Eq. (4.16b) is a more suitable form to use when J is calculated on a desk calculator since K and $\Lambda_0(\psi, k)$ are tabulated in Ref. (7). The dashed lines in Fig. A-1 are lines of constant J in the b-c plane.

The submergence ratio $(H-h)/C_h$ is calculated from Eqs (4.17), (4.22), (4.26b) and (4.33). The exact part of the M integral as given in Eq. (4.33) is easily evaluated by the methods described in Ref. (8).

Since the integral part of M is always less than two percent of the total M, (at least for the range of cases that we calculated) the numerical integration need not be done to a great degree of accuracy. When the integral is divided into three appropriately chosen intervals it converges very rapidly to the desired accuracy of a total of five significant figures in M or at most three figures in the integral part.

The spray-sheet contraction, δ/d requires the calculation of the I integral as well as the M integral. The I integral as given in Eq. (4.25) is divided into two integrals I_1 and I_2, where I_1, the more lengthy calculation, is independent of c and hence independent of C_h/h.

B. Finite Bottom

In order to calculate the lift slope for this case the parameter b' must be evaluated from Eq. (4.10) for each prescribed ℓ (or B') and any set of C_h/h, b, and c calculated as outlined above. We chose to do only one case where b = c and hence Eq. (4.10) could be solved directly for b' rather than by iteration.

The lift slope, C_{L_α} is now readily obtained from Eq. (3.5) in which

$$\theta_1 = \frac{a}{\pi}\sqrt{\frac{(c+1)(b'+c)}{c}}\ J'$$

and

$$\theta_2 = \frac{a}{\pi}\sqrt{\frac{(b-1)(b'-b)}{b}}\ J' ,$$

where

$$J' = -\int_0^{-1}\sqrt{\frac{t}{(1-t)(b'-t)}}\ \frac{dt}{t+c}$$

and

$$J' = \int_0^1 \sqrt{\frac{t}{(1-t)(b'-t)}}\ \frac{dt}{b-t}$$

J^* and J' can be reduced to elliptic integrals with the following results:

$$J^* = 2k^*\left[\Pi\left(-\frac{1}{c},\ k^*\right) - K(k^*)\right]$$

or in alternate form

$$J^* = \pi\sqrt{\frac{c}{(1+c)(b'+c)}}\ \Lambda_0(\psi',\ k^*) - \frac{2\sqrt{b'}}{b'+c}\ ;$$

and for J' we find

$$J' = 2k^*\left[\Pi\left(\frac{1}{b},\ k^*\right) - K(k^*)\right]$$

or

$$J' = k\,k^*\ \frac{1 - \Lambda_0(\theta,\ k^*)}{\sqrt{(k^2 - k^{*2})(1 - k^2)}}$$

where

$$k^2 = \frac{1}{b}\ ,\qquad k^{*2} = \frac{1}{b'}\ ,$$

$$\psi' = \sin^{-1}\sqrt{\frac{b'}{b'+c}}\ ,$$

and

$$\theta = \sin^{-1}\sqrt{\frac{1 - k^2}{1 - k^{*2}}}\ .$$

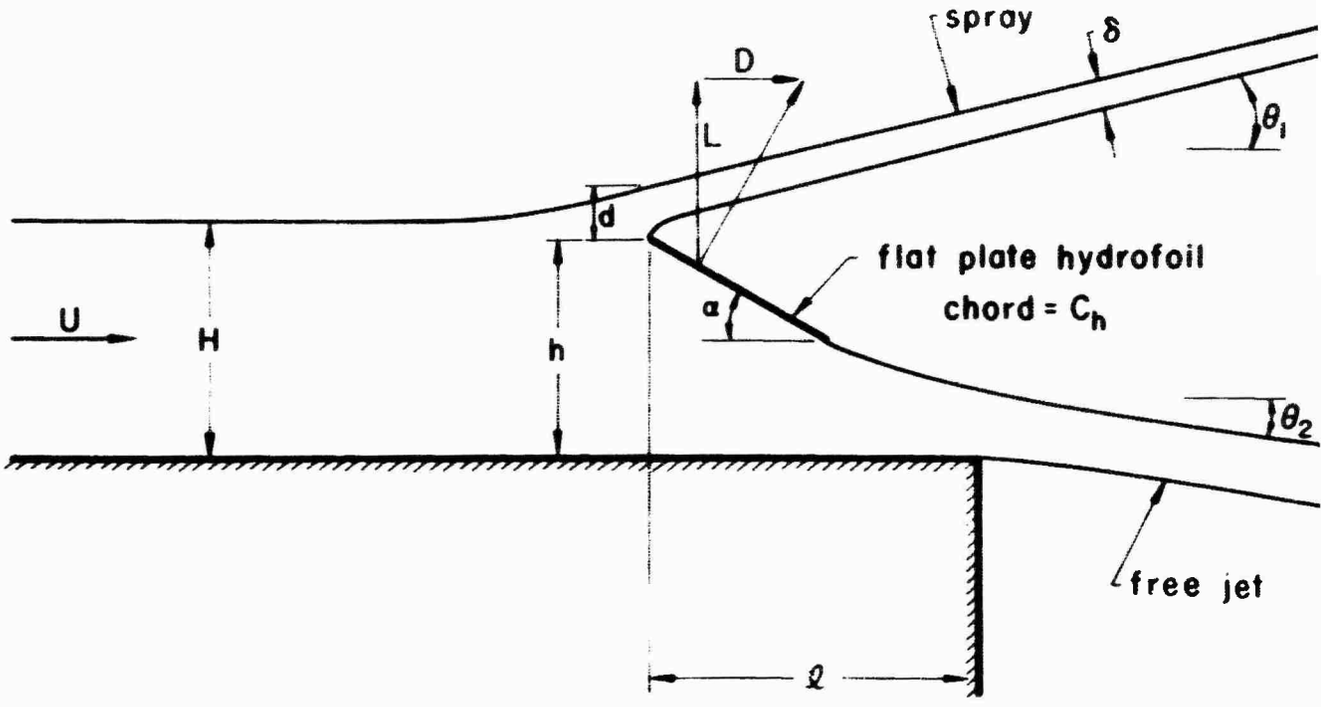

Figure 1. Sketch showing a cavitating flat plate in a stream of finite depth with the lower surface partly free and partly solid.

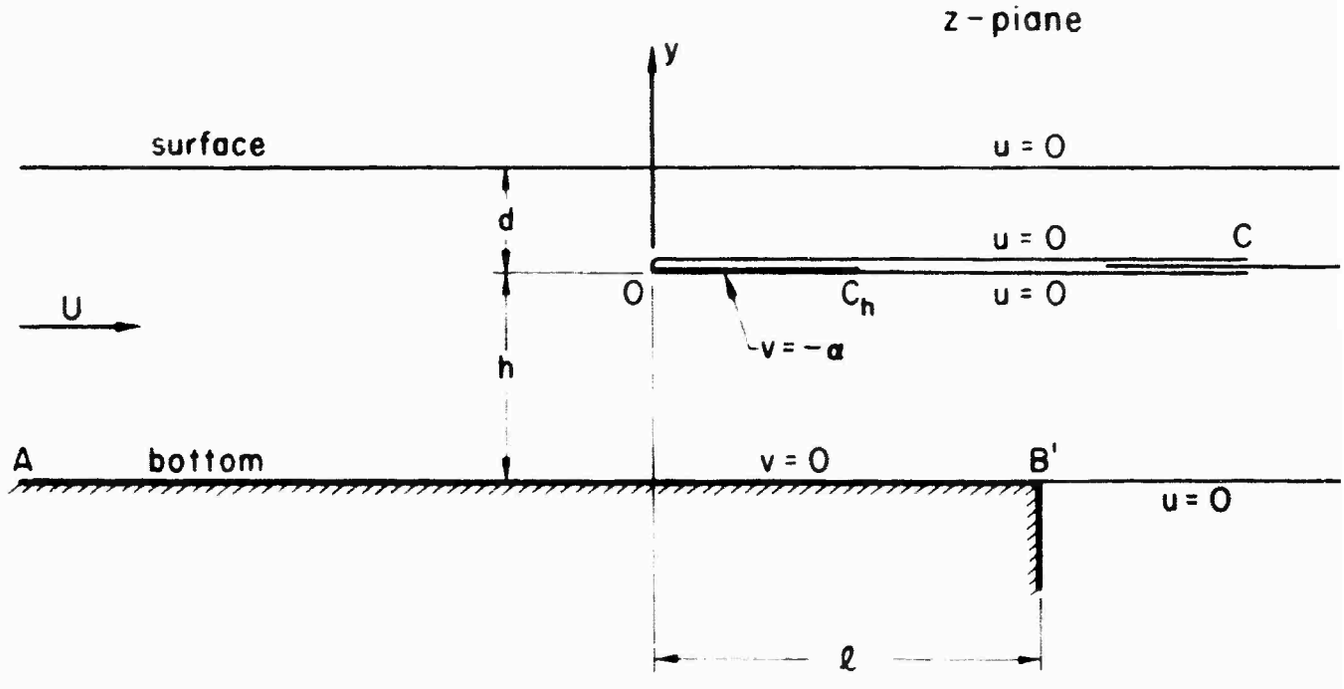

Figure 2. Diagram of the physical z-plane showing boundary conditions for the linearized flow.

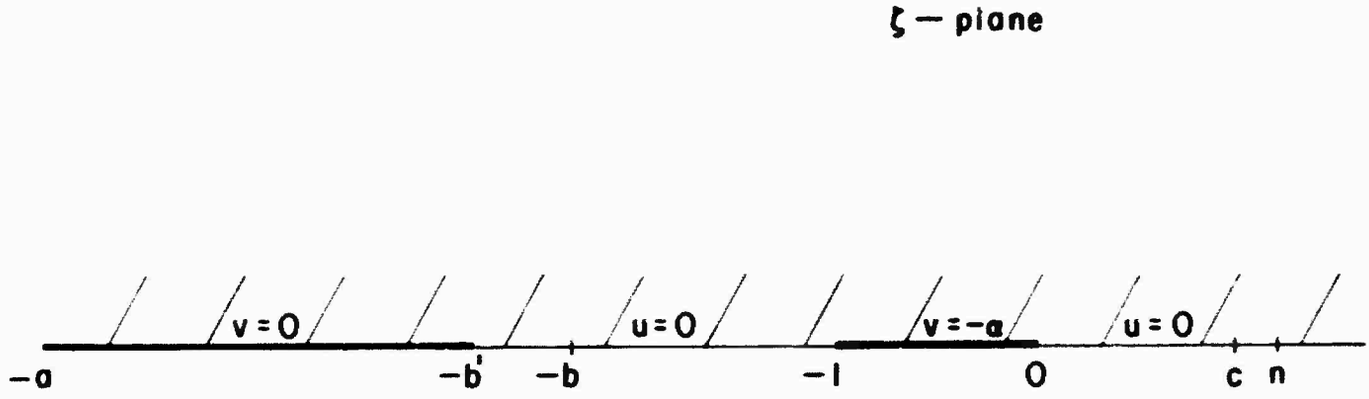

Figure 3. The auxiliary ζ-plane.

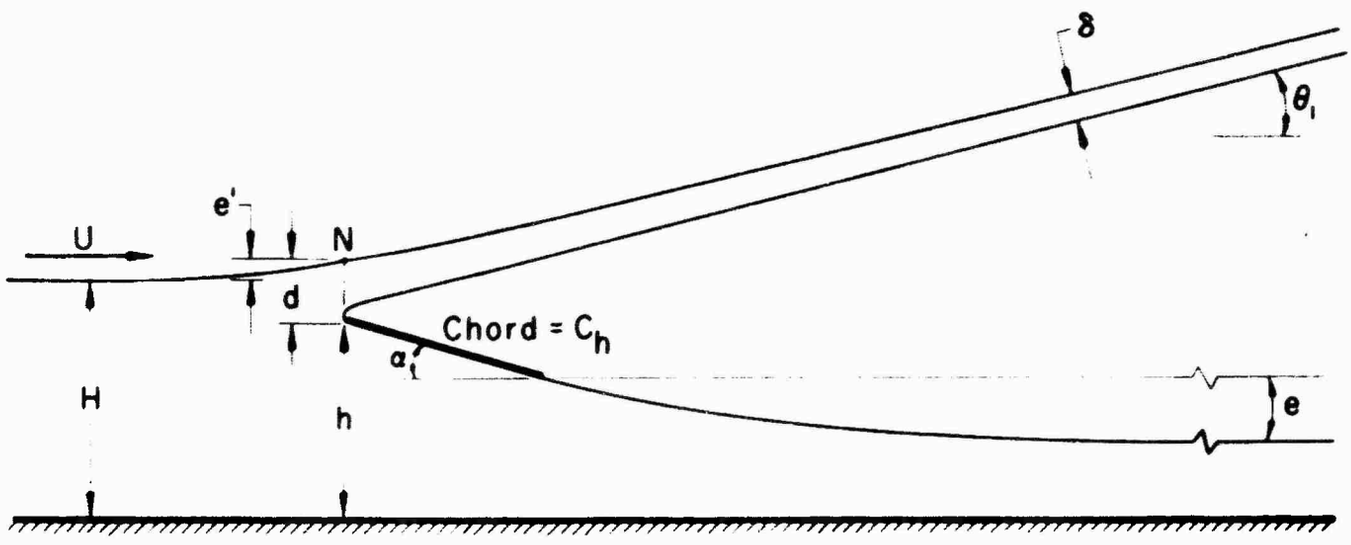

Figure 4. Definition sketch of a cavitating flat plate in a stream of finite depth.

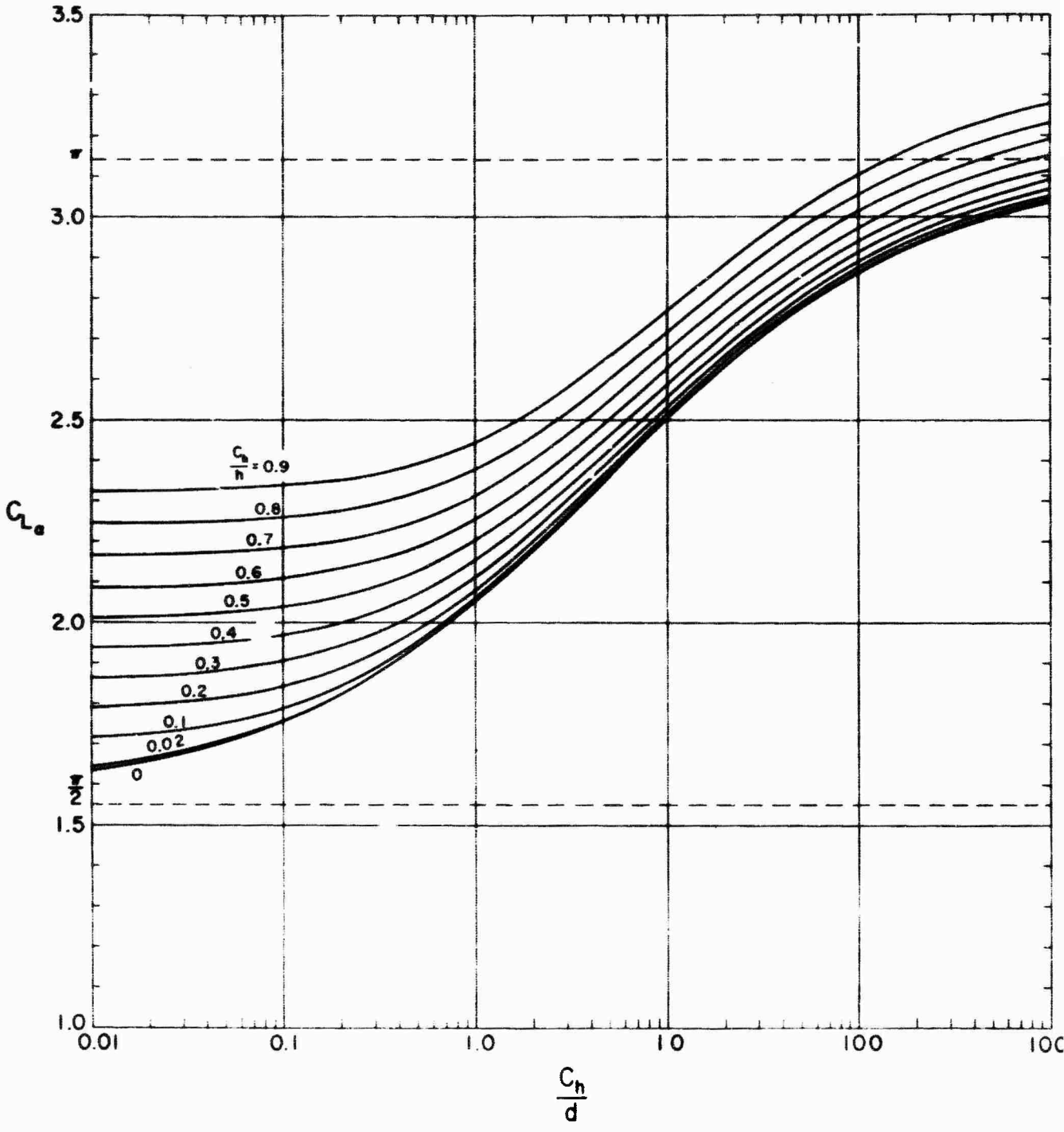

Figure 5. The lift slope C_{L_α} versus C_h/d for various values C_h/h for a flat plate hydrofoil in a stream of finite depth.

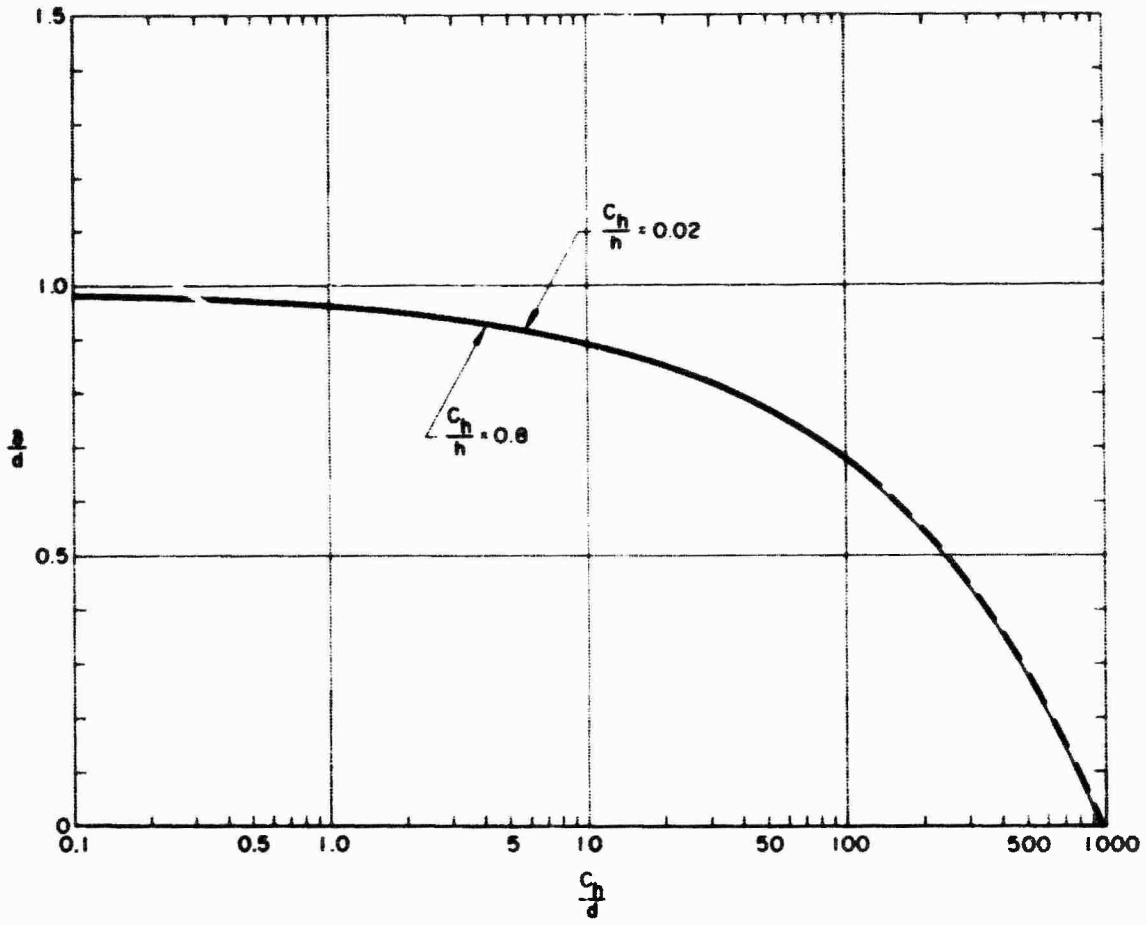

Figure 6. The spray sheet contraction δ/d versus C_h/d for various values of C_h/h at an angle of attack of 6°.

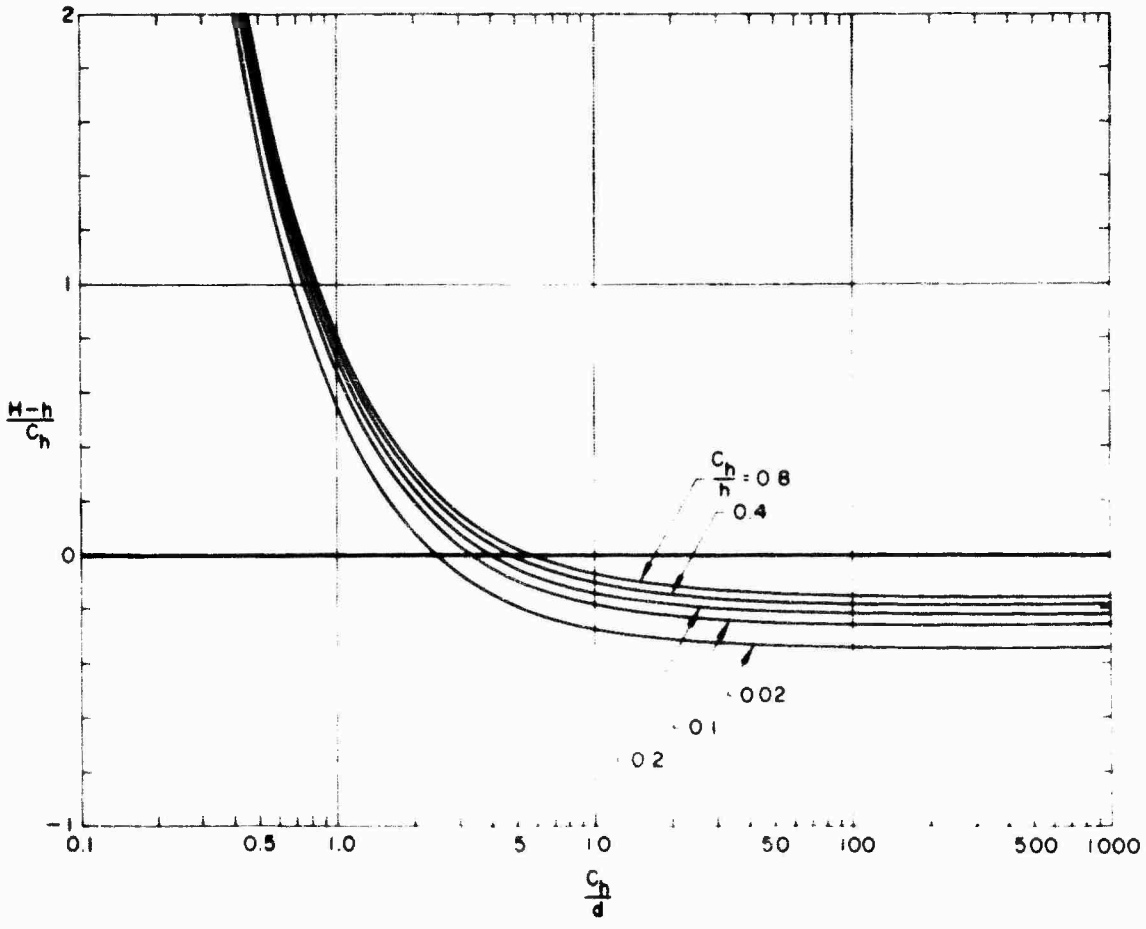

Figure 7. Submergence of the plate versus C_h/d for several values of C_h/h at an angle of attack of 6°.

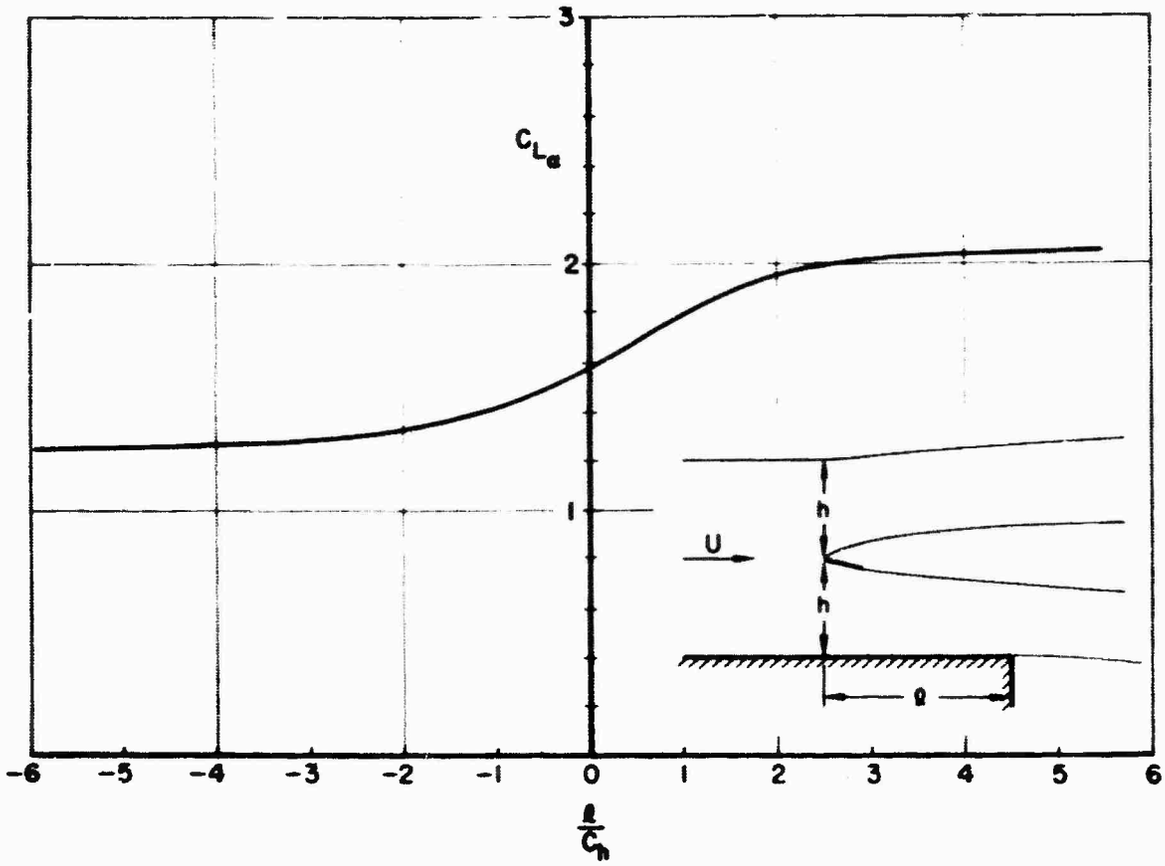

Figure 8. The lift slope C_{L_α} versus various length of bottom wall with the hydrofoil midway between top and bottom surfaces and for the chord-depth ratio of 0.4.

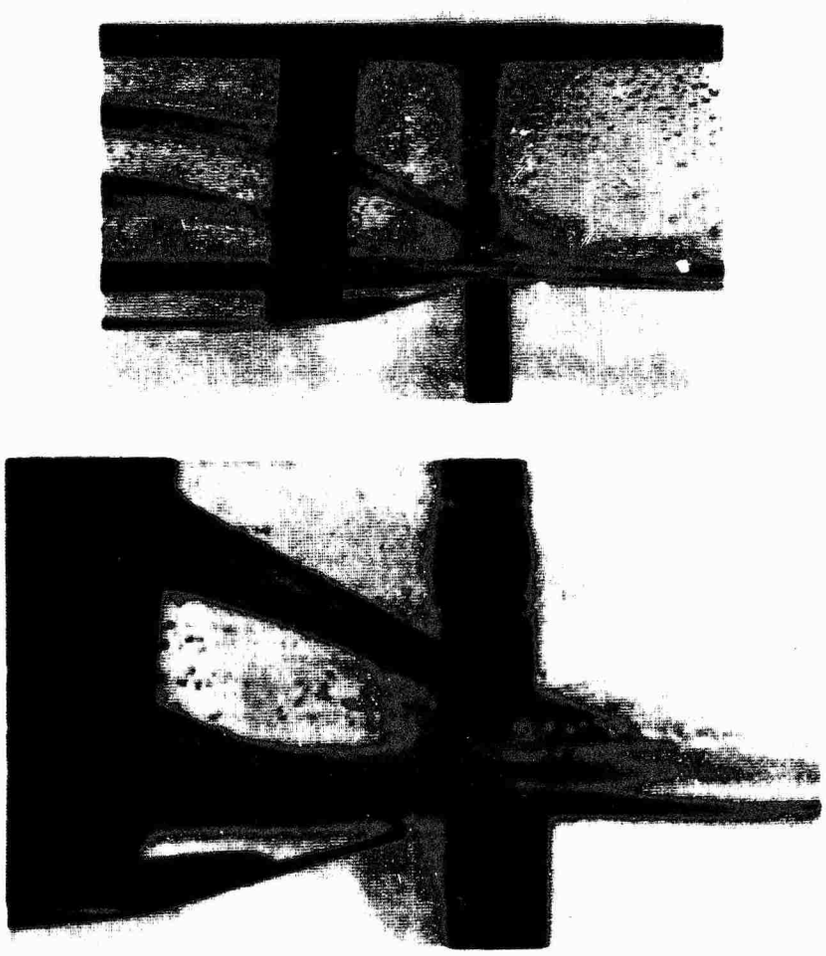

Figure 9. Two photographs of the planing flat plate at an angle of attack of about twenty degrees at a velocity of about 12 ft. per sec.

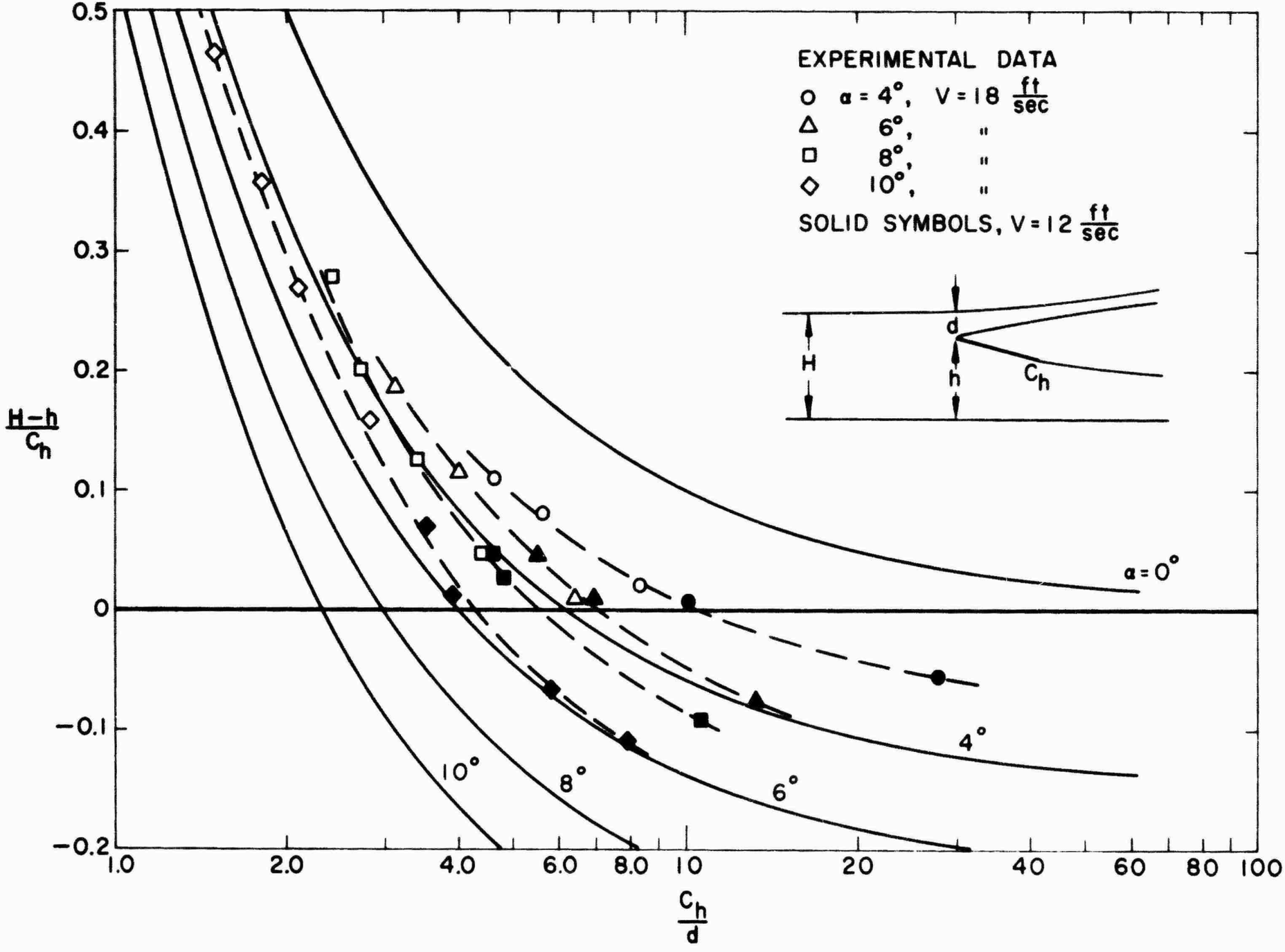

Figure 10. Submergence of the plate versus spray sheet thickness at the leading edge for various angles of attack. The solid lines are the theory evaluated for a value of $C_h/h = 0.2$.

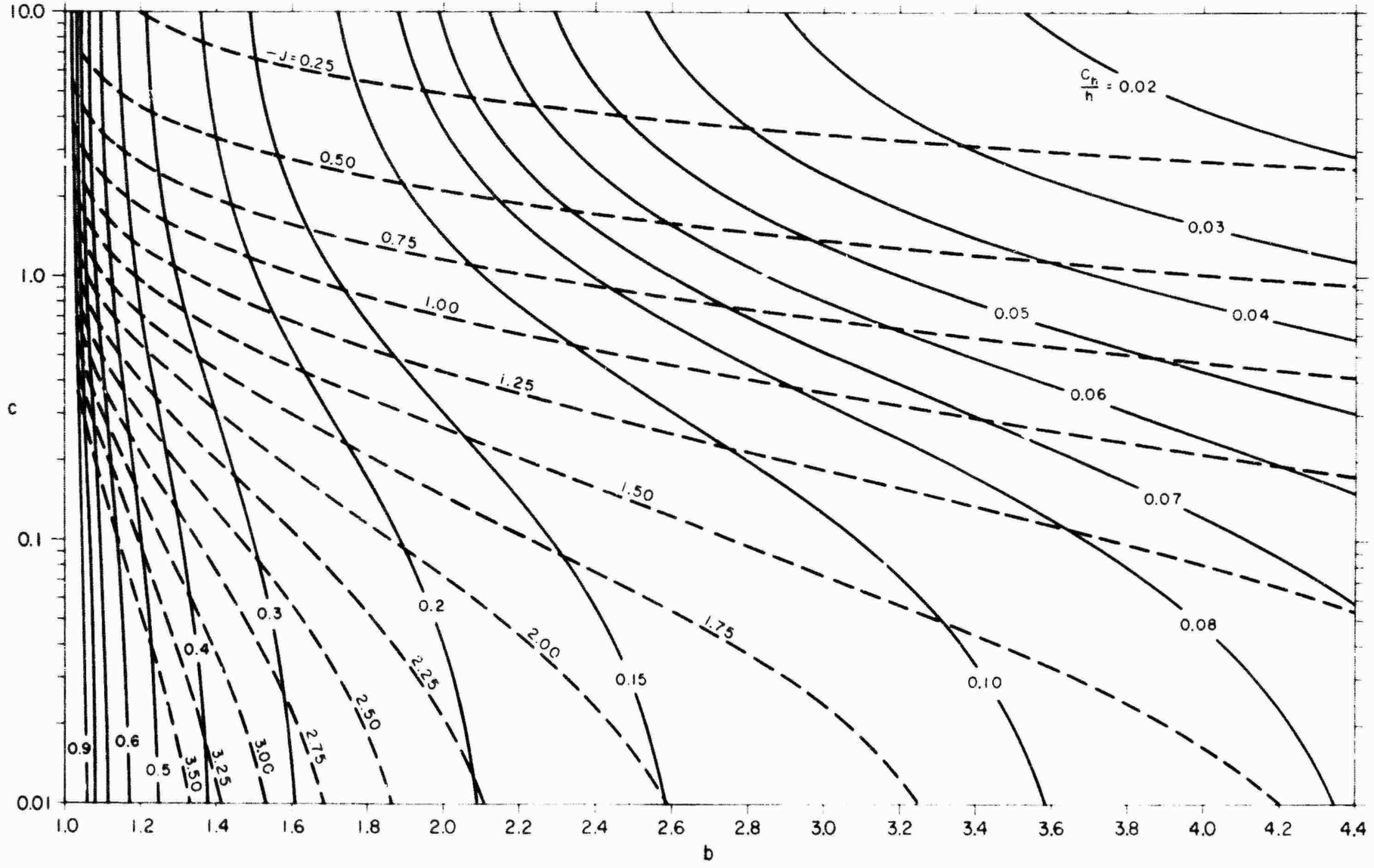

Figure A-1. Graph of the parameters of the mapping function for various values of chord-depth ratio and the J integral.

TABLE 1

$C_h/h = 0.02$

b	c	-J	M	I
3.46	1.32717 × 10	6.8351 × 10^{-8}	9.181	3.690
3.50	1.11699 × 10	7.9669 × 10^{-8}	8.765	3.722
3.55	9.64373	9.9531 × 10^{-8}	8.424	3.755
3.60	8.48661	1.0099 × 10^{-7}	8.201	3.787
3.9	6.83960	1.2979 × 10^{-7}	7.885	3.850
4.00	5.83394	1.8764 × 10^{-7}	7.377	4.090
4.5	3.13649	2.1535 × 10^{-7}	7.307	4.203
4.7	2.2784	2.6260 × 10^{-7}	7.301	
5.0	1.87621	2.9258 × 10^{-7}	7.355	4.568
5.5	1.42916	3.3503 × 10^{-7}	7.499	
6.0	1.13382	3.7062 × 10^{-7}	7.670	5.017
7.0	7.63772 × 10^{-1}	4.2824 × 10^{-7}	8.038	5.401
8.0	5.39231 × 10^{-1}	4.7434 × 10^{-7}	8.403	5.732
9.0	3.85 - × 10^{-1}	5.1330 × 10^{-7}	8.751	6.022
10.0	2.79002 × 10^{-1}	5.4759 × 10^{-7}	9.080	6.278
11.0	1.98065 × 10^{-1}	5.7883 × 10^{-7}	9.388	6.503
12.0	1.37194 × 10^{-1}	6.0821 × 10^{-7}	9.676	6.705
13.0	8.95378 × 10^{-2}	6.3684 × 10^{-7}	9.944	6.884
14.0	5.27273 × 10^{-2}	6.6608 × 10^{-7}	10.191	7.046
15.0	2.44454 × 10^{-2}	6.9832 × 10^{-7}	10.414	7.186
15.5	1.39595 × 10^{-2}	7.1737 × 10^{-7}		
16.0	5.18424 × 10^{-3}	7.4168 × 10^{-7}	10.593	7.312
16.2	3.71757 × 10^{-3}	7.4782 × 10^{-7}	10.606	7.323
16.2	2.36772 × 10^{-3}	7.5503 × 10^{-7}	10.616	7.335
16.25	1.74313 × 10^{-3}	7.5923 × 10^{-7}	10.619	
16.30	1.15811 × 10^{-3}	7.6401 × 10^{-7}	10.622	7.345
16.32	9.36889 × 10^{-4}	7.6619 × 10^{-7}	10.622	
16.34	7.24121 × 10^{-4}	7.6858 × 10^{-7}	10.622	
16.36	5.20999 × 10^{-4}	7.7127 × 10^{-7}	10.621	
16.38	3.29463 × 10^{-4}	7.7441 × 10^{-7}	10.619	
16.40	1.53067 × 10^{-4}	7.7841 × 10^{-7}	10.615	

$C_h/h = 0.04$

b	c	-J
2.40	6.18222 × 10	1.9692 × 10^{-8}
2.45	2.12739 × 10	5.4072 × 10^{-8}
2.5	1.28163 × 10	8.8063 × 10^{-8}
2.6	7.10395	1.4782 × 10^{-6}
2.65	5.79538	1.7499 × 10^{-1}
2.7	4.84632	2.0057 × 10^{-8}
2.75	4.21759	2.2472 × 10^{-8}
2.8	3.70467	2.4755 × 10^{-8}
2.85	3.29854	2.6918 × 10^{-8}
2.9	2.96880	2.8971 × 10^{-8}
2.95	2.69558	3.0923 × 10^{-8}
3.0	2.46539	3.2782 × 10^{-8}
3.05	2.26870	3.4555 × 10^{-8}
3.1	2.09861	3.6249 × 10^{-8}
3.3	1.59843	4.2341 × 10^{-8}
3.4	1.41974	4.5039 × 10^{-8}
3.5	1.27186	4.7545 × 10^{-8}
3.6	1.14732	4.9882 × 10^{-8}
3.7	1.04090	5.2069 × 10^{-8}
3.8	9.48846 × 10^{-2}	5.4125 × 10^{-8}
3.9	8.68369 × 10^{-2}	5.6062 × 10^{-8}
4.0	7.97379 × 10^{-2}	5.7894 × 10^{-8}
4.1	7.34261 × 10^{-2}	5.9631 × 10^{-8}
4.2	6.77753 × 10^{-2}	6.1282 × 10^{-8}
4.3	6.26854 × 10^{-2}	6.2857 × 10^{-8}
4.5	5.38818 × 10^{-2}	6.5803 × 10^{-8}
4.7	4.65298 × 10^{-2}	6.8517 × 10^{-8}
5.0	3.75294 × 10^{-2}	7.2237 × 10^{-8}

$C_h/h = 0.03$

b	c	-J
2.75	3.01569 × 10	3.6118 × 10^{-8}
2.80	1.80194 × 10	5.8719 × 10^{-8}
2.85	1.23414 × 10	8.0090 × 10^{-8}
2.90	9.96939	1.0033 × 10^{-7}
2.95	8.14218	1.1955 × 10^{-7}
3.00	6.47684	1.3781 × 10^{-7}
3.05	5.56832	1.5519 × 10^{-7}
3.10	5.23730	1.7176 × 10^{-7}
3.15	4.67528	2.4694 × 10^{-7}
3.20	4.21959	2.0270 × 10^{-7}
3.25	3.84248	2.1718 × 10^{-7}
3.30	3.52510	2.3105 × 10^{-7}
3.35	3.25418	2.4436 × 10^{-7}
3.40	3.02012	2.5715 × 10^{-7}
3.45	2.81580	2.6945 × 10^{-7}
3.5	2.63581	2.8128 × 10^{-7}
3.6	2.34311	3.0369 × 10^{-7}
3.7	2.08820	3.2458 × 10^{-7}
3.8	1.88574	3.4412 × 10^{-7}
3.9	1.71549	3.6245 × 10^{-7}
4.0	1.56993	3.7971 × 10^{-7}
4.1	1.44419	3.9600 × 10^{-7}
4.2	1.33410	4.1142 × 10^{-7}
4.3	1.23739	4.2605 × 10^{-7}
4.4	1.15122	4.3997 × 10^{-7}
4.5	1.07407	4.5327 × 10^{-7}
4.7	9.41558 × 10^{-1}	4.7803 × 10^{-7}
4.8	8.84191 × 10^{-1}	4.6566 × 10^{-7}
4.9	8.31712 × 10^{-1}	5.0082 × 10^{-7}

$C_h/h = 0.05$

b	c	-J
2.2	4.07365 × 10	3.1747 × 10^{-8}
2.3	9.53669	1.2359 × 10^{-8}
2.4	5.33805	2.0220 × 10^{-8}
2.5	3.67054	2.7036 × 10^{-8}
2.6	2.77285	3.3012 × 10^{-8}
2.7	2.21038	3.8306 × 10^{-8}
2.8	1.82397	4.3036 × 10^{-8}
2.9	1.54156	4.7298 × 10^{-8}
3.0	1.32575	5.1164 × 10^{-8}
3.1	1.15520	5.4695 × 10^{-8}
3.2	1.01684	5.7940 × 10^{-8}
3.3	9.22134 × 10^{-1}	6.0937 × 10^{-8}
3.4	8.05615 × 10^{-1}	6.3719 × 10^{-8}
3.5	7.23040 × 10^{-1}	6.6314 × 10^{-8}
3.6	6.51603 × 10^{-1}	6.8745 × 10^{-8}
3.7	5.89170 × 10^{-1}	7.1032 × 10^{-8}
3.8	5.34125 × 10^{-1}	7.3190 × 10^{-8}
3.9	4.85226 × 10^{-1}	7.5235 × 10^{-8}
4.0	4.41500 × 10^{-1}	7.7179 × 10^{-8}
4.5	2.77982 × 10^{-1}	8.5718 × 10^{-8}

TABLE I (cont'd.)

$C_h/h = 0.2$

b	c	-J	M	I
1.340	1.19396 × 10	1.8039 × 10^{-2}		
1.345	3.24024 × 10	6.4779 × 10^{-3}		
1.350	1.86942 × 10	1.1012 × 10^{-2}		
1.36	1.00022 × 10	1.9685 × 10^{-3}		
1.37	6.76154	2.7868 × 10^{-3}		
1.38	5.06817	3.5602 × 10^{-3}		
1.40	3.32306	4.9861 × 10^{-3}		
1.45	1.63009	7.9766 × 10^{-3}		
1.50	1.06438	1.0352	9.303	4.161
1.55	7.37706 × 10^{-2}	1.2290	9.058	
1.6	5.35291 × 10^{-2}	1.3905	8.932	4.283
1.65	3.98592 × 10^{-2}	1.5280	8.870	
1.7	3.00535 × 10^{-2}	1.6470	8.847	4.394
1.75	2.27205 × 10^{-2}	1.7519	8.848	
1.8	1.70725 × 10^{-2}	1.8460	8.866	4.495
1.85	1.26312 × 10^{-2}	1.9320	8.894	
1.9	9.09181 × 10^{-3}	2.0121	8.929	4.586
1.95	6.24959 × 10^{-3}	2.0886	8.966	
2.0	3.97102 × 10^{-3}	2.1643	9.004	4.667
2.05	2.16695 × 10^{-2}	2.2431	9.037	
2.10	7.93707 × 10^{-3}	2.3346	9.057	4.739
2.11	5.71768 × 10^{-3}	2.3567	9.057	4.745
2.12	3.69533 × 10^{-3}	2.3816		
2.13	1.89790 × 10^{-3}	2.4116	9.047	
2.132	1.57005 × 10^{-3}	2.4187	9.044	
2.134	1.25456 × 10^{-3}	2.4263	9.041	
2.136	9.52710 × 10^{-4}	2.4346	9.037	
2.138	6.66439 × 10^{-4}	2.4442	9.033	
2.139	5.30052 × 10^{-4}	2.4493	9.030	
2.14	3.98905 × 10^{-4}	2.4551	9.027	4.764

$C_h/h = 0.3$

b	c	-J	M	I
1.216	1.05110 × 10	2.2383 × 10^{-3}		
1.218	8.88030	2.6070 × 10^{-3}		
1.220	7.67496	2.9700 × 10^{-3}		
1.225	5.09909	3.8459 × 10^{-3}		
1.23	4.50335	4.6815 × 10^{-3}		
1.24	3.12758	6.2426 × 10^{-3}		
1.25	2.35930	7.6721 × 10^{-3}	11.816	4.103
1.30	9.39653 × 10^{-1}	1.3325	10.323	4.172
1.35	5.01739 × 10^{-1}	1.7309	9.841	4.236
1.40	2.9219 × 10^{-1}	2.0292	9.635	4.296
1.45	1.71951 × 10^{-1}	2.2649	9.543	4.351
1.50	9.62856 × 10^{-2}	2.4614	9.506	4.402
1.52	7.39345 × 10^{-2}	2.5432		
1.55	4.66448 × 10^{-2}	2.6373	9.494	4.448
1.56	3.89766 × 10^{-2}	2.6717		
1.58	2.55301 × 10^{-2}	2.7417		
1.60	1.44284 × 10	2.8162	9.479	4.490
1.61	9.72891 × 10^{-3}	2.8572		
1.62	5.61600 × 10^{-3}	2.9034	9.458	4.505
1.625	3.79755 × 10^{-3}	2.9299		
1.630	2.16047 × 10^{-3}	2.9609		
1.632	1.56445 × 10^{-3}	2.9753		
1.634	1.00869 × 10^{-3}	2.9919		
1.635	7.48489 × 10^{-4}	3.0014	9.413	4.513
1.636	5.02476 × 10^{-4}	3.0122		

$C_h/h = 0.4$

b	c	-J	M	I
1.135	5.06709 × 10	5.6981 × 10^{-3}		
1.136	3.01033 × 10	9.4670 × 10^{-3}		
1.137	2.13489 × 10	1.3177 × 10^{-2}		
1.138	1.65908 × 10	1.6831 × 10^{-2}		
1.140	1.12925 × 10	2.3978 × 10^{-2}	20.852	
1.145	6.21051	4.0099 × 10^{-2}		
1.150	4.21274	5.6625 × 10^{-2}	15.194	4.130
1.160	2.48202	8.4939 × 10^{-2}	13.376	4.144
1.180	1.25844	1.3155	11.875	4.172
1.200	7.74661 × 10^{-2}	1.6831	11.209	4.199
1.220	5.17512 × 10^{-2}	1.9607	10.837	4.224
1.240	3.59400 × 10^{-2}	2.2270	10.604	4.248
1.260	2.53467 × 10^{-2}	2.4351	10.449	4.270
1.280	1.78480 × 10^{-2}	2.6147	10.340	4.292
1.30	1.23444 × 10^{-2}	2.7729	10.262	4.313
1.32	8.25322 × 10^{-3}	2.9156	10.203	4.333
1.34	5.07974 × 10^{-3}	3.0489	10.154	4.352
1.35	3.81098 × 10^{-3}	3.1139	10.132	4.360
1.36	2.71342 × 10^{-3}	3.1793	10.110	
1.38	9.84331 × 10^{-4}	3.3202	10.054	
1.385	6.46929 × 10^{-4}	3.3612	10.036	
1.390	3.50812 × 10^{-4}	3.4084	10.012	
1.392	2.45354 × 10^{-4}	3.4304	9.999	
1.394	1.48641 × 10^{-4}	3.4556	9.840	
1.396	6.27545 × 10^{-6}	3.4875	9.963	

$C_h/h = 0.5$

b	c	-J	M	I
1.091	1.34287 × 10^{2}	2.4318 × 10^{-2}		
1.092	3.57619 × 10	8.9529 × 10^{-3}		
1.093	2.04875 × 10	1.5323 × 10^{-2}		
1.094	1.42867 × 10	2.1548 × 10^{-2}		
1.095	1.09259 × 10	2.7632 × 10^{-2}		
1.0975	6.80696	4.2255 × 10^{-2}		
1.10	4.88739	5.6091 × 10^{-2}	17.559	4.175
1.11	2.16829	1.0470	14.369	4.187
1.12	1.30460	1.4462	13.138	4.200
1.13	8.82394 × 10^{-2}	1.7797	12.470	4.212
1.14	6.33408 × 10^{-2}	2.0624	12.048	4.224
1.15	4.70140 × 10^{-2}	2.3090	11.756	4.235
1.16	3.55561 × 10^{-2}	2.5159	11.543	4.246
1.17	2.71314 × 10^{-2}	2.7011	11.381	4.257
1.18	2.07270 × 10^{-2}	2.8657	11.254	4.268
1.19	1.57393 × 10^{-2}	3.0136	11.151	4.278
1.20	1.17866 × 10^{-2}	3.1482	11.065	4.287
1.21	8.61751 × 10^{-3}	3.2723	10.992	4.297
1.22	6.06038 × 10^{-3}	3.3888	10.928	4.305
1.23	3.99676 × 10^{-3}	3.5007	10.869	4.314
1.24	2.34594 × 10^{-3}	3.6121	10.810	4.322
1.25	1.05980 × 10^{-3}	3.7310	10.744	4.329
1.255	5.50146 × 10^{-4}	3.7945	10.702	4.331
1.260	1.41948 × 10^{-5}	3.8885	10.643	4.336
1.262	1.93698 × 10^{-6}	3.9491	10.598	

TABLE I (cont'd.)

$C_h/h = 0.06$

b	c	-J
2.05	3.29725 × 10	4.1340 × 10^{-2}
2.10	1.25219 × 10	1.0292 × 10^{-2}
2.15	7.67374	1.5906 × 10^{-3}
2.20	5.50083	2.1047 × 10^{-3}
2.25	4.26644	2.5774 × 10^{-3}
2.30	3.46973	3.0139 × 10^{-3}
2.35	2.91245	3.4184 × 10^{-3}
2.40	2.50043	3.7944 × 10^{-3}
2.45	2.18314	4.1451 × 10^{-3}
2.50	1.93119	4.4732 × 10^{-3}
2.55	1.72592	4.7809 × 10^{-3}
2.60	1.55552	5.0703 × 10^{-3}
2.65	1.41168	5.3432 × 10^{-3}
2.70	1.28856	5.6010 × 10^{-3}
2.75	1.18194	5.8452 × 10^{-3}
2.80	1.08866	6.0770 × 10^{-3}
2.85	1.00634	6.2974 × 10^{-3}
2.9	9.33137 × 10^{-1}	6.5074 × 10^{-3}
2.95	8.67584 × 10^{-2}	6.7078 × 10^{-3}
3.0	8.08530 × 10^{-1}	6.8995 × 10^{-3}
3.05	7.55043 × 10^{-1}	7.0830 × 10^{-3}
3.1	7.06360 × 10^{-1}	7.2591 × 10^{-3}
3.2	6.21012 × 10^{-1}	7.5909 × 10^{-3}
3.3	5.48616 × 10^{-1}	7.8990 × 10^{-3}
3.4	4.86422 × 10^{-1}	8.1864 × 10^{-3}
3.5	4.32418 × 10^{-1}	8.4559 × 10^{-3}
3.6	3.85099 × 10^{-1}	8.7098 × 10^{-3}
3.7	3.43314 × 10^{-1}	8.9501 × 10^{-3}
3.8	3.06173 × 10^{-1}	9.1784 × 10^{-3}
3.9	2.72969 × 10^{-1}	9.3964 × 10^{-3}
4.0	2.43140 × 10^{-1}	9.6052 × 10^{-3}
4.2	1.91867 × 10^{-1}	1.0000
4.5	1.31231 × 10^{-1}	1.0550

$C_h/h = 0.07$

b	c	-J
1.95	1.81769 × 10	7.6863 × 10^{-2}
2.00	8.68016	1.5074 × 10^{-3}
2.05	5.65014	2.1753 × 10^{-3}
2.10	4.15766	2.7819 × 10^{-3}
2.15	3.26828	3.3356 × 10^{-3}
2.20	2.67727	3.8433 × 10^{-3}
2.25	2.25565	4.3108 × 10^{-3}
2.30	1.93943	4.7431 × 10^{-3}
2.35	1.69328	5.1442 × 10^{-3}
2.40	1.49609	5.5177 × 10^{-3}
2.5	1.19949	6.1935 × 10^{-3}
2.6	9.86672 × 10^{-1}	6.7901 × 10^{-3}
2.7	8.26270 × 10^{-1}	7.3223 × 10^{-3}
2.8	7.00894 × 10^{-1}	7.8016 × 10^{-3}
2.9	6.00124 × 10^{-1}	8.2370 × 10^{-3}
3.0	5.17330 × 10^{-1}	8.6354 × 10^{-3}
3.1	4.48095 × 10^{-1}	9.0028 × 10^{-3}
3.2	3.89359 × 10^{-1}	9.3437 × 10^{-3}
3.3	3.38935 × 10^{-1}	9.6622 × 10^{-3}
3.4	2.95216 × 10^{-1}	9.9615 × 10^{-3}
3.5	2.56999 × 10^{-1}	1.0244
3.6	2.23360 × 10^{-1}	1.0513
3.7	1.93581 × 10^{-1}	1.0770
3.8	1.67097 × 10^{-1}	1.1017
3.9	1.43455 × 10^{-1}	
4.0	1.22289 × 10^{-1}	1.1469
4.1	1.03302 × 10^{-1}	1.1717
4.3	7.09372 × 10^{-2}	1.2165
4.5	4.49010 × 10^{-2}	1.2619

$C_h/h = 0.08$

b	c	-J
1.85	1.84186 × 10	7.9393 × 10^{-2}
1.9	7.98817	1.6995 × 10^{-3}
2.0	3.64367	3.2346 × 10^{-3}
2.1	2.29653	4.489[illegible] × 10^{-3}
2.2	1.63798	5.5363 × 10^{-3}
2.3	1.24629	6.4267 × 10^{-3}
2.4	9.85936 × 10^{-2}	7.1957 × 10^{-3}
2.5	8.00005 × 10^{-2}	7.8691 × 10^{-3}
2.6	6.60404 × 10^{-2}	8.4659 × 10^{-3}
2.7	5.51663 × 10^{-2}	9.0018 × 10^{-3}
2.8	4.64556 × 10^{-2}	9.4846 × 10^{-3}
2.9	3.93239 × 10^{-2}	9.9270 × 10^{-3}
3.0	3.33829 × 10^{-2}	1.0334
3.1	2.83641 × 10^{-2}	1.0713
3.2	2.40763 × 10^{-2}	1.1067
3.3	2.03796 × 10^{-2}	1.1401
3.4	1.71687 × 10^{-2}	1.1719
3.5	1.43642 × 10^{-2}	1.2023
3.6	1.1 041 × 10^{-2}	1.2317
3.7	9.73987 × 10^{-2}	1.2604
3.8	7.83337 × 10^{-2}	1.2887
3.9	6.15436 × 10^{-2}	1.3169
4.0	4.67919 × 10^{-2}	1.3454
4.1	3.38985 × 10^{-2}	1.3750
4.2	2.27384 × 10^{-2}	1.4064
4.3	1.32518 × 10^{-2}	1.4413
4.4	5.49070 × 10^{-2}	1.4841

$C_h/h = 0.1$

b	c	-J	M	I
1.70	1.88252 × 10	8.4116 × 10^{-2}	15.096	3.816
1.710	1.39783 × 10	1.1112 × 10^{-3}	13.545	
1.73	9.18236	1.6286 × 10^{-3}	11.793	
1.75	6.80277	2.1176 × 10^{-3}	10.810	
1.80	4.07078	3.2308 × 10^{-3}	9.555	3.940
1.85	2.86001	4.2109 × 10^{-3}	8.956	
1.90	2.17576	5.0811 × 10^{-3}	8.616	4.057
2.0	1.42803	6.5611 × 10^{-3}	8.275	4.167
2.1	1.02652	7.7768 × 10^{-3}	8.138	4.271
2.2	7.75420 × 10^{-1}	8.7979 × 10^{-3}	8.095	4.370
2.3	6.03353 × 10^{-1}	9.6724 × 10^{-3}	8.103	4.464
2.4	4.78059 × 10^{-1}	1.0434	8.141	4.553
2.5	3.82828 × 10^{-1}	1.1108	8.198	4.638
2.6	3.08133 × 10^{-1}	1.1712	8.265	4.718
2.8	1.99098 × 10^{-1}	1.2768	8.437	4.867
3.0	1.24439 × 10^{-1}	1.3686	8.606	4.998
3.2	7.15849 × 10^{-2}	1.4514	8.775	5.122
3.4	3.39988 × 10^{-2}	1.5382	8.932	5.2[illegible]
3.5	1.98169 × 10^{-2}	1.5846	9.002	
3.6	8.48678 × 10^{-3}	1.6392	9.060	
3.62	6.57732 × 10^{-3}	1.6522	9.069	
3.64	4.79880 × 10^{-3}	1.6665	9.076	
3.66	3.16334 × 10^{-3}	1.6827	9.081	
3.68	1.69313 × 10^{-3}	1.7023	9.082	
3.685	1.35613 × 10^{-3}	1.7080	9.081	
3.695	7.[illegible]650 × 10^{-4}	1.7215	9.077	
3.698	5.53264 × 10^{-4}	1.7264	9.075	

TABLE 1 (cont'd.)

$C_h/h = 0.6$

b	c	-J	M	I
1.064	3.31678×10	1.8620×10^{-2}		
1.065	1.63592×10	2.0905×10^{-2}		
1.070	4.39808	6.7581×10^{-3}		
1.075	2.40034	1.0754	16.654	4.218
1.080	1.58367	1.4210		4.224
1.085	1.14018	1.7226	14.054	4.229
1.090	8.62526×10^{-1}	1.9879	13.569	4.235
1.095	6.72979×10^{-1}	2.2230	13.183	4.240
1.10	5.35829×10^{-1}	2.4327	12.905	4.245
1.11	3.51875×10^{-1}	2.7911		
1.12	2.35650×10^{-1}	3.0868	12.235	4.264
1.130	1.56976×10^{-1}	3.3365	12.034	4.272
1.140	1.01474×10^{-1}	3.5526	11.877	4.281
1.150	6.12582×10^{-2}	3.7454	11.746	4.289
1.160	3.21041×10^{-2}	3.9255		
1.165	2.08250×10^{-2}	4.0153		
1.170	1.15006×10^{-2}	4.1097		
1.175	4.12279×10^{-3}	4.2191		
1.1775	1.27595×10^{-3}	4.2928		

$C_h/h = 0.7$

b	c	-J	M	I
1.046	1.47316×10	2.5158×10^{-2}		
1.049	4.72175	6.9414×10^{-3}		
1.05	3.79768	8.2883×10^{-3}		
1.0525	2.49532	1.1411		
1.055	1.81265	1.4224		
1.060	1.10961	1.9084		
1.065	7.52085×10^{-1}	2.3129		
1.070	5.37116×10^{-1}	2.6545		
1.075	3.94700×10^{-1}	2.9466		
1.080	2.94251×10^{-1}	3.1995		
1.085	2.20288×10^{-1}	3.4210		
1.090	1.64145×10^{-1}	3.6171	14.467	4.277
1.100	8.63535×10^{-2}	3.9527	12.708	4.284
1.105	5.91986×10^{-2}	4.1005		
1.110	3.76651×10^{-2}	4.2406		
1.115	2.07742×10^{-2}	4.3785		
1.1175	1.38794×10^{-2}	4.4498		
1.120	7.98035×10^{-3}	4.5262	12.274	4.294
1.121	5.90684×10^{-3}	4.5595		
1.122	4.00833×10^{-3}	4.5957		
1.123	2.30292×10^{-3}	4.6368		

$C_h/h = 0.8$

b	c	-J	M	I
1.0320	5.47192×10	7.6728×10^{-2}		
1.0325	2.01206×10	2.0259×10^{-2}		
1.0330	1.22061×10	3.2429×10^{-3}	30.843	
1.0340	6.71653	5.5595×10^{-3}	24.944	
1.035	4.55847	7.7314×10^{-3}	22.131	
1.040	1.57844	1.6816	17.297	4.269
1.045	8.46716×10^{-1}	2.3697	15.763	4.272
1.050	5.20095×10^{-1}	2.9071	14.971	4.276
1.055	3.37806×10^{-1}	3.3377	14.473	4.279
1.060	2.23440×10^{-1}	3.6707	14.124	4.283
1.065	1.46544×10^{-1}	3.9866	13.854	4.286
1.070	9.26389×10^{-2}	4.2407	13.644	4.288
1.075	5.40290×10^{-2}	4.4656	13.460	4.290
1.080	2.63750×10^{-2}	4.6746	13.290	4.292
1.082	1.78032×10^{-2}	4.7581	13.220	4.294
1.084	1.05262×10^{-2}	4.8452	13.147	4.294
1.086	4.55558×10^{-3}	4.9429	13.062	4.294
1.0865	3.28478×10^{-3}	4.9712	13.036	4.294
1.087	2.11656×10^{-3}	5.0026	13.008	4.294
1.08725	1.57584×10^{-3}	5.0202	12.992	4.294
1.0875	1.06866×10^{-3}	5.0398	12.974	4.294
1.08775	6.01408×10^{-4}	5.0628	12.953	4.294
1.088	1.88429×10^{-4}	5.0936	12.924	4.294

$C_h/h = 0.9$

b	c	-J	M
1.023	4.84568×10	9.2912×10^{-2}	59.413
1.0235	1.53590×10	2.8124×10^{-2}	
1.024	8.99324	4.6095×10^{-3}	29.596
1.0245	6.29044	6.3261×10^{-3}	26.216
1.025	4.79589	7.9672×10^{-3}	24.110
1.030	1.21719	2.1091	17.770
1.035	5.73821×10^{-1}	3.0112	16.190
1.040	3.11648×10^{-1}	3.6653	15.414
1.045	1.73797×10^{-1}	4.1613	14.929
1.050	9.22167×10^{-2}	4.5542	14.580
1.055	4.13876×10^{-2}	4.8833	14.295
1.0575	2.37190×10^{-2}	5.0363	14.161
1.060	1.02074×10^{-2}	5.1935	14.019
1.0605	7.98235×10^{-3}	5.2273	13.988
1.0610	5.92171×10^{-3}	5.2630	13.954
1.0615	4.03433×10^{-3}	5.3015	13.918
1.062	2.33771×10^{-3}	5.3447	13.877
1.0625	8.71556×10^{-4}	5.3986	13.824

TABLE 2

b=c=1.182302

$C_h/h = 0.4$

b'	J^*	J'	C_{L_α}	L/C_h
1.183	1.3606	9.2919	2.05	5.36
1.185	1.3562	9.2542	2.04	4.29
1.190	1.3452	9.1620	2.03	3.45
1.200	1.3243	8.9863	2.01	2.79
1.220	1.2856	8.6656	1.97	2.18
1.250	1.2344	8.2471	1.91	1.70
1.300	1.1627	7.6738	1.84	1.25
1.400	1.0533	6.8260	1.74	0.72
1.500	0.9718	6.2166	1.66	0.39
2.00	0.7417	4.5869	1.49	0.50
3.00	0.5509	3.3292	1.38	-1.35
4.00	0.4584	2.7450	1.34	-1.87
6.00	0.3609	2.1440	1.30	-2.55
8.00	0.3073	1.8174	1.29	-3.03
10.00	0.2722	1.6074	1.28	-3.39
15.00	0.2194	1.2922	1.27	-4.04
20.00	0.1888	1.1106	1.26	-4.50
30.00	0.1532	0.9001	1.254	-5.15
50.00	0.1181	0.6931	1.250	-5.96
100.00	0.0832	0.4880	1.25	-7.06